Balanced Excitation and Inhibition are Required for High-Capacity, Noise-Robust Neuronal Selectivity

Ran Rubin⋆

Department of Neuroscience
Columbia University
New York NY 10027 USA

L. F. Abbott

Department of Neuroscience
Department of Physiology and Cellular Biophysics
Columbia University
New York NY 10027 USA

and

Haim Sompolinsky

Edmond and Lily Safra Center for Brain Sciences
Racah Institute of Physics
The Hebrew University of Jerusalem,
Edmond J. Safra Campus
Jerusalem 9190401, Israel

Center for Brain Science
Harvard University
Cambridge MA 02138, USA

⋆ For correspondence: rr2980@columbia.edu

1

Abstract

Neurons and networks in the cerebral cortex must operate reliably despite multiple sources of noise. To evaluate the impact of both input and output noise, we determine the robustness of single-neuron stimulus selective responses, as well as the robustness of attractor states of networks of neurons performing memory tasks. We find that robustness to output noise requires synaptic connections to be in a balanced regime in which excitation and inhibition are strong and largely cancel each other. We evaluate the conditions required for this regime to exist and determine the properties of networks operating within it. A plausible synaptic plasticity rule for learning that balances weight configurations is presented. Our theory predicts an optimal ratio of the number of excitatory and inhibitory synapses for maximizing the encoding capacity of balanced networks for a given statistics of afferent activations. Previous work has shown that balanced networks amplify spatio-temporal variability and account for observed asynchronous irregular states. Here we present a novel type of balanced network that amplifies small changes in the impinging signals, and emerges automatically from learning to perform neuronal and network functions robustly.

Introduction

The response properties of neurons in many brain areas including cerebral cortex are shaped by the balance between co-activated inhibitory and excitatory synaptic inputs [1, 2, 3, 4, 5] (for a review see [6]). Excitation-inhibition balance may have different forms in different brain areas or species and its emergence likely arise from multiple mechanisms. Theoretical work has shown that, when externally driven, circuits of recurrently connected excitatory and inhibitory neurons with strong synapses settle rapidly into a state in which population activity levels ensure a balance of excitatory and inhibitory currents [7, 8]. Experimental evidence in some systems indicates that synaptic plasticity plays a role in maintaining this balance [9, 10, 11, 12]. Here we address the question of what computational benefits are conferred by the excitation-inhibition balance properties of balanced and unbalanced neuronal circuits. Although it has been shown that networks in the balanced states have advantages in generating fast and linear response to changing stimuli, [13, 7, 8, 14], the advantages and disadvantages of excitation-inhibition balance for general information processing have not been elucidated (except in special architectures; see [15, 16]). Here we compare the computational properties of neurons operating with and without excitation-inhibition balance and present a constructive computational reason for strong, balanced excitation and inhibition: it is needed for neurons to generate selective responses that are robust to output noise, and it is crucial for the stability of memory states in associative memory networks. The novel balanced networks we present naturally and automatically emerge from synaptic learning that endows neurons and networks with robust functionality.

We begin our analysis by considering a single neuron receiving input from a large number of afferents. We characterize its basic task as discriminating patterns of input activation to which it should respond by firing action potentials from other patterns which should leave it quiescent. Neurons implement this form of response selectivity by applying a threshold to the sum of inputs from their presynaptic afferents. The simplest (parsimonious) model that captures these basic elements is the binary model neuron [17, 18], which has been studied extensively [19, 20, 21, 22] and used to model a variety of neuronal circuits [23, 24, 25, 26, 27]. Our work is based on including and analyzing the implications of four fundamental neuronal features not previously considered together: 1) non-negative input, corresponding to the fact that neuronal activity is characterized by firing rates; 2) a membrane potential threshold for neuronal firing above the resting potential (and hense a silent resting state); 3) sign-constrained and bounded synaptic weights, meaning that individual synapses are either excitatory or inhibitory and the total synaptic strength is limited; and 4) two sources of noise, input and output noise, representing fluctuations arising from variable stimuli and inputs and from processes within the neuron. As will be shown, these features imply that, when the number of input afferents is large, synaptic input must be strong and balanced if the neuron's response selectivity is to be robust. We extend our analysis to recurrently connected networks storing long-term memory and find that similar balanced synaptic patterns are required for the stability of the memory states against noise. In addition, maximizing the performance of neurons and networks in the balanced state yields a prediction for the optimal ratio of excitatory to inhibitory inputs in cortical circuits.

Results

Our model neuron is a binary unit that is either active or quiescent depending on whether its membrane potential is above or below a firing threshold. The potential, labeled V_{PSP}, is a weighted sum of inputs x_i, $i = 1, 2, ..., N$, that represent afferent firing rates and are thus non-negative,

$$V_{\text{PSP}} \left(\boldsymbol{x}, \ \boldsymbol{w} \right) = V_{\text{rest}} + \sum_{i=1}^{N} w_i x_i \, , \tag{1}$$

where V_{rest} is the resting potential of the neuron and $\boldsymbol{x}$ and $\boldsymbol{w}$ are N-component vectors with elements x_i and w_i respectively. The weight w_i represents the synaptic efficacy of the i'th input. If $V_{\text{PSP}} \geq V_{\text{th}}$ the neuron is in an active state, otherwise, it is in a quiescent state. To implement the segregation of excitatory and inhibitory inputs, each weight is constrained so that $w_i \geq 0$ if input i is excitatory and $w_i \leq 0$ if input i is inhibitory.

To function properly in a circuit, a neuron must respond selectively to an appropriate set of inputs. To characterize selectivity, we define a set of P exemplar input vectors $\boldsymbol{x}^\mu$, with $\mu = 1, 2, ..., P$, and randomly assign them to two classes, denoted as 'plus' and 'minus'. The neuron must respond to inputs belonging to the 'plus' class by firing (active state) and to the 'minus' class by remaining quiescent. This means that the neuron is acting as a perceptron [17, 18, 19, 20, 21, 28, 24, 26]. We assume the P input activations, $\boldsymbol{x}^\mu$, are drawn i.i.d. from a distribution with non-negative means, $\bar{\boldsymbol{x}}$, and covariance matrix, C (when N is large, higher moments of the distribution of $\boldsymbol{x}$ have negligible effect). For simplicity we assume that the stimulus average activities are the same for all input neurons within a population, so that $\bar{x}_i = \bar{x}_{\text{exc(inh)}} \geq 0$, and that C is diagonal with equal variances within a population, $\sigma_i^2 = \sigma_{\text{exc(inh)}}^2$. Note that synaptic weights are in units of membrane potential over input activity levels (firing rates), and hence will be measured in units of $(V_{\text{th}} - V_{\text{rest}}) / \sigma_{\text{exc}}$.

We call weight vectors that correctly categorize the P exemplar input patterns, $\boldsymbol{x}^\mu$ for $\mu = 1, 2, ..., P$, solutions of the categorization task presented to the neuron. Before describing in detail the properties of the solutions, we outline a broad distinction between two types of possible solutions. One type is characterized by weak synapses, *i.e.*, individual synaptic weights that are inversely proportional to the total number of synaptic inputs, $w_i \sim 1/N$ (note that weights weaker than $\mathcal{O}\left(1/N\right)$ will not enable the neuron to cross threshold). For this solution type, the total excitatory and inhibitory parts of the membrane potential are of the same order as the neuron's threshold. An alternative scenario is a solution in which individual synaptic weights are relatively strong, $w_i \sim 1/\sqrt{N}$. In this case, both the total excitatory and inhibitory parts of the potential are, individually, much greater than the threshold, but they make approximately equal contributions, so that excitation and inhibition tend to cancel, and the mean V_{PSP} is close to threshold. We call the first type of solution *unbalanced* and the second *balanced*. Note that the norm of the weight vector, $|\boldsymbol{w}| = \sqrt{\sum_{i=1}^{N} w_i^2}$, serves to distinguish the two types of solutions. This norm is of order of $1/\sqrt{N}$ for unbalanced solutions and of order 1 in the balanced case. Weights with norms stronger than $\mathcal{O}\left(1\right)$ lead to membrane potential values that are much larger in magnitude than the neuron's threshold. For biological neurons postsynaptic potentials of such magnitude can result in very high, unreasonable firing rates (although see [29]). We therefore impose an upper bound of the weight norm $|\boldsymbol{w}| \leq \Gamma$

where Γ is of order 1. We now argue that the differences between unbalanced and balanced solutions have important consequences for the way the system copes with noise.

As mentioned above, neurons in the central nervous system are subject to multiple sources of noise, and their performance must be robust to its effects. We distinguish two biologically relevant types of noise: *input noise* resulting from the fluctuations of the stimuli and sensory processes that generate the stimulus related input $\boldsymbol{x}$; and *output noise* arising from afferents unrelated to a particular task or from biophysical processes internal to the neuron, including fluctuations in the effective threshold due to spiking history and adaptation [30, 31, 32] (For theoretical modeling see [33]). Both sources of noise result in trail-by-trial fluctuations of the membrane potential V_{PSP} and, for a robust solution, the probability of changing the state of the output neuron relative to the noise-free condition must be low. The two sources of noise differ in their dependence on the magnitude of the synaptic weights. Because input noise is filtered through the same set of synaptic weights as the signal, its effect on the membrane potential is sensitive to the magnitude of those weights. Specifically, if the trial-to-trial variability of each input x_i^{μ} is characterized by standard deviation σ_{in}, the fluctuations it generates in the membrane potential have standard deviation $|\boldsymbol{w}|\sigma_{\text{in}}$ (Fig. 1 top row). On the other hand, the effect of output noise is independent of the synaptic weights $\boldsymbol{w}$. Output noise characterized by standard deviation σ_{out} induces membrane potential fluctuations with the same standard deviation σ_{out} for both types of solutions (Fig. 1 bottom row).

We can now appreciate the basis for the difference in the noise robustness of the two types of solutions. For unbalanced solutions, the difference between the potential induced by typical 'plus' and 'minus' noise-free inputs (the signal) is of the order of $|\boldsymbol{w}| = \mathcal{O}\left(1/\sqrt{N}\right)$ (Fig. 1 left column). Although the fluctuations induced by input noise are of this same order (Fig. 1 top left), output noise yields fluctuations in the membrane potential of order 1, which is much larger than the magnitude of the weak signal (Fig. 1 bottom left). In contrast, for balanced solutions, the signal differentiating 'plus' and 'minus' patterns is of order $|\boldsymbol{w}| = \mathcal{O}(1)$, which is the same order as the fluctuations induced by both types of noise (Fig. 1 right column). Thus, we are led to the important observation that the balanced solution provides the only hope for producing selectivity that is robust against both types of noise. However, there is no guaranty that robust, balanced solutions exist or that they can be found and maintained in a manner that can be implemented by a biological system. A key question, therefore, is under what conditions does a balanced solution to the selectivity task exist and what are, in detail, its robustness properties. Below, we derive conditions for the existence of a balanced solution, analyze its properties, and study the implications for single-neuron and network computation. We show that, subject to a small reduction of the total information stored in the network, robust and balanced solutions exist and can emerge naturally when learning occurs in the presence of output noise.

Balanced and unbalanced solutions

We begin by presenting the results of an analytic approach [19, 21, 20] for determining existence conditions and analyzing properties of weights that generate a specified selectivity, independent of the particular method or learning algorithm used to find the weights (*SI Methods*). We
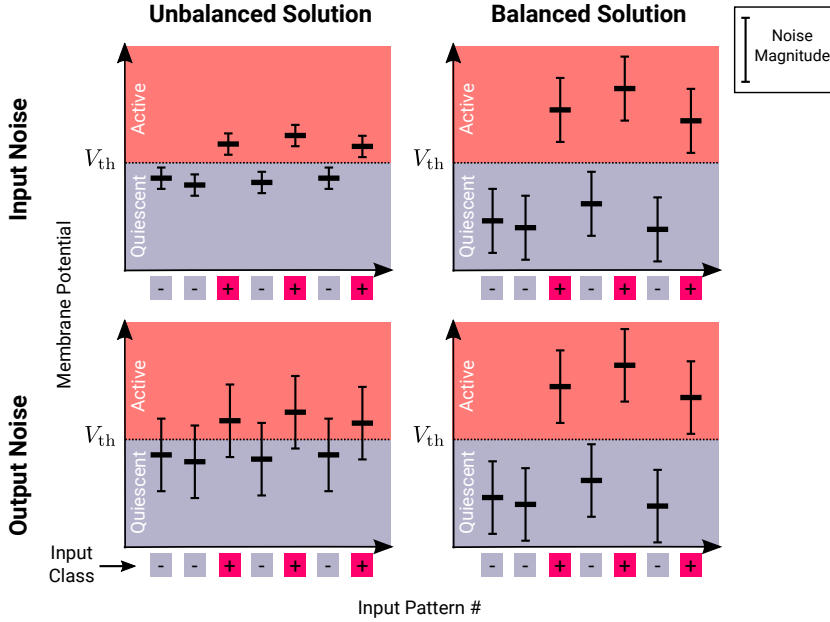
Figure 1: **Only balanced solutions can be robust to both input and output noise.** Each panel depicts membrane potentials resulting from different input patterns in a classification task. Weights are unbalanced ($|\boldsymbol{w}| = \mathcal{O}\left(1/\sqrt{N}\right)$, left column) or balanced ($|\boldsymbol{w}| = \mathcal{O}(1)$, right column). The neuron is in an active state only if the membrane potential is greater than the threshold V_{th}. The input pattern class ('plus' or 'minus') is specified by the squares underneath the horizontal axis. Each input pattern determines a membrane potential (mean, horizontal bars) that fluctuates from one presentation to another due to input noise (top row) and output noise (bottom row). Vertical bars depict the magnitude of the noise in each case. The variability of the mean V_{PSP} across input patterns (which is the signal differentiating input pattern classes) is proportional to $|\boldsymbol{w}|$. As a result, the mean V_{PSP}'s for unbalanced solutions (left column) cluster close to the threshold (difference from threshold $\mathcal{O}\left(1/\sqrt{N}\right)$). For balanced solutions (right column), the mean V_{PSP}'s have a larger spread (potential difference $\mathcal{O}(1)$). Input noise (fluctuations of x_i, top row) produces membrane potential fluctuations with standard deviation that is proportional to $|\boldsymbol{w}|$, which is of $\mathcal{O}\left(1/\sqrt{N}\right)$ for unbalanced solutions (top left) and of $\mathcal{O}(1)$ for balanced solutions (top right). Output noise (bottom row) produces membrane potential fluctuation that are independent of $|\boldsymbol{w}|$, so it is of the same magnitude for both solution types. Thus, while both balanced and unbalanced solutions can be robust to input noise, only balanced solutions can also be robust to substantial output noise.

validate the theoretical results by using numerical methods that can determine the existence of such weights and find them if they exist (*Methods*).

When the number of patterns P is too large, solutions may not exist. The maximal value of P that permits solutions is proportional to the number of synapses, N, so a useful measure is the ratio $\alpha = P/N$, which we call the load. The capacity, denoted as α_c, is the maximal load that permits solutions to the task. The capacity depends on the relative number of 'plus' and 'minus' input patterns. For simplicity we assume throughout that the two classes are equal in size (but see *SI Methods*). A classic result for the perceptron with weights that are not sign constrained is that the capacity is $\alpha_c = 2$ [34, 35, 19]. For the 'constrained perceptron' considered here, we find that α_c depends also on the fraction of excitatory afferents, denoted by f_{exc}. This fraction is an important architectural feature of neuronal circuits and varies in different brain systems. For $f_{exc} = 0$, namely purely inhibitory circuit, the capacity vanishes, because when all the input to the neuron is inhibitory, V_{PSP} cannot reach threshold and the neuron is quiescent for all stimuli. When the circuit includes excitatory synapses, the task can be solved by appropriate shaping of the strength of the excitatory and inhibitory synapses, and this ability increases the larger the fraction of excitatory synapses is. Therefore, For $f_{exc} > 0$, α_c increases with f_{exc} up to a maximum of $\alpha_c = 1$ (half the capacity of an unconstrained perceptron) for fractions equal or greater than a critical fraction $f_{exc} = f_{exc}^\star$. This dependence can be summarized by the capacity curve $\alpha_c (f_{exc})$ (Fig. 2a, black line) bounding the range of loads which admit solutions for the different excitatory/inhibitory ratios.

Interestingly, $f_{exc}^\star$ depends on the statistics of the inputs (*SI Methods*). We denote the coefficient of variation (CV) of the excitatory and inhibitory input activities by $CV_{exc} = \sigma_{exc}/\bar{x}_{exc}$ and $CV_{inh} = \sigma_{inh}/\bar{x}_{inh}$, respectively. These, measure the degree of stimulus tuning of the two afferent populations. In terms of these quantities, the critical excitatory fraction is

$$f_{exc}^\star = \frac{CV_{exc}}{CV_{exc} + CV_{inh}} \; . \tag{2}$$

In other words, the critical ratio between the number of excitatory and inhibitory afferents ($f_{exc}^\star/(1\text{-}f_{exc}^\star)$) equals the ratio of their degree of tuning. To understand the origin of this result, we note that to maximize the encoding capacity, the relative strength of the weights should be inversely proportional to the standard deviation of their afferents, $\bar{w}_{exc(inh)} \propto 1/\sigma_{exc(inh)}$, implying that the mean total synaptic inputs is proportional to $f_{exc}\bar{w}_{exc}\bar{x}_{exc} + f_{inh}\bar{w}_{inh}\bar{x}_{inh} = f_{exc}/CV_{exc} - f_{inh}/CV_{inh}$ where $f_{inh} = 1 - f_{exc}$. For excitatory fraction $f_{exc} > f_{exc}^\star$ this mean total synaptic inputs is positive, allowing the voltage to reach the threshold and the neuron to implement the required selectivity task with optimally scaled weights. Thus, the capacity of the neuron is unaffected by changes in f_{exc} in the range $f_{exc}^\star \leq f_{exc} \leq 1$. For excitatory fraction $f_{exc} < f_{exc}^\star$ the neuron cannot remain responsive (reach threshold) with optimally scaled weights, and thus the capacity is reduced.

In cortical circuits, inhibitory neurons tend to fire at higher firing rates and are thought to be more broadly tuned than excitatory neurons [4, 36, 37], implying $f_{exc}^\star > 0.5$ (*SI Methods*). This is consistent with the abundance of excitatory synapses in cortex. However, input statistics that make $f_{exc}^\star < 0.5$ do not change the qualitative behavior we discuss (*SI Methods* and Fig. S2a).

For load levels below the capacity, many synaptic weight vectors solve the selectivity task and
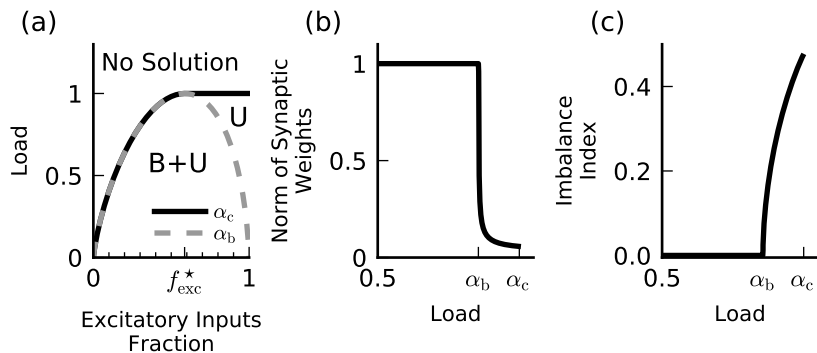
Figure 2: **Balanced and unbalanced solutions.** (a) Perceptron solutions as a function of load and fraction of excitatory weights. Above the capacity line ($\alpha_{\mathrm{c}}(f_{\mathrm{exc}})$, black line) no solution exists. Balanced solutions exist only below the balanced capacity line, ($\alpha_{\mathrm{b}}(f_{\mathrm{exc}})$, dashed gray line). Between the balanced capacity and maximum capacity lines, only unbalanced solutions exist (U). On the other hand, below the balanced capacity line, unbalanced solutions coexist with balanced ones (B+U). (b) The norm of the synaptic weight vector of typical solutions as a function the load (in units of $(V_{\mathrm{th}} - V_{\mathrm{rest}})/\sigma_{\mathrm{exc}}$). Below α_{b} the norm is clipped at its upper bound Γ (in this case $\Gamma = 1$). Above α_{b} the norm collapses and is of order $1/\sqrt{N}$ (shown here for $N = 3000$). (c) The input imbalance index (IB, eq. 3) of typical solutions as a function of the load. Note the sharp onset of imbalance above α_{b}. In (b) and (c) $f_{\mathrm{exc}} = 0.8$, yielding $\alpha_{\mathrm{c}} = 1$. See *Methods* for other parameters used. For simulation results see Fig. S1.

8

we now describe the properties of the different solutions. In particular, we investigate the parameter regimes where balanced or unbalanced solutions exist. We find that unbalanced solutions with weights vector norm of order $1/\sqrt{N}$ exist for all load values below α_{c}. As for the balanced solutions with weight vector norms of order 1, they exist below a critical value α_{b} which may be smaller than α_{c}. Specifically, for $f_{\mathrm{exc}} \leq f^{\star}_{\mathrm{exc}}$ balanced solutions exist for all load values below capacity, *i.e.*, $\alpha_{\mathrm{b}} = \alpha_{\mathrm{c}}$. For $f_{\mathrm{exc}} > f^{\star}_{\mathrm{exc}}$, α_{b} is smaller than α_{c} and decreases with f_{exc} until it vanishes at $f_{\mathrm{exc}} = 1$ (Fig. 2a, dashed gray line). The absence of balanced solutions for $f_{\mathrm{exc}} = 1$ is clear, as there is no inhibition to balance the excitatory inputs. Furthermore, the synaptic excitatory weights must be weak (scaling as $1/N$) to ensure that V_{PSP} remains close to threshold (slightly above it for 'plus' patterns and slightly below it for 'minus' ones). For $1 \geq f_{\mathrm{exc}} > f^{\star}_{\mathrm{exc}}$ the predominance of excitatory afferents precludes a balanced solution if the load is high, i.e., $\alpha_{\mathrm{b}} \leq \alpha \leq \alpha_{\mathrm{c}}$. As argued above and shown below, the balanced solution is more robust than the unbalanced solution. Hence, we can identify $f^{\star}_{\mathrm{exc}}$ as the optimal fraction of excitatory input, because it is the fraction of excitatory afferents for which the capacity of *balanced* solutions is maximal.

For loads below α_{b} both balanced and unbalanced solutions exist, raising the question what would be the character of a weight vector that is sampled randomly from the space of all possible solutions. Our theory predicts that whenever the balance solution exists, the vast majority of the solutions are balanced and furthermore have a weight vector norm that is saturated at the upper bound Γ. Thus, for $f_{\mathrm{exc}} > f^{\star}_{\mathrm{exc}}$, the *typical* solution undergoes a transition from balanced to unbalanced weights as α crosses the balanced capacity line $\alpha_{\mathrm{b}}(f_{\mathrm{exc}})$. At this point the norm of the solution collapses from Γ to $|\boldsymbol{w}| \sim 1/\sqrt{N}$ (Fig. 2b).

As explained above, for balanced solutions we expect to find a near cancellation of the total excitatory and inhibitory inputs. Our theory confirms this expectation. To measure the degree of E-I cancellation for any solution, we introduce the *imbalance index*,

$$\mathrm{IB} = \frac{\sum_i w_i \bar{x}_i}{\sum_{i \in \mathrm{exc}} w_i \bar{x}_i - \sum_{i \in \mathrm{inh}} w_i \bar{x}_i} \ , \tag{3}$$

where the bar symbol denotes an average over all the input patterns (μ). Whereas for the unbalanced solution the IB is of order 1, for the balanced solution it is small, of order $1/\sqrt{N}$. Thus, the typical solution below α_{b} has zero imbalance (to leading order in N), but the imbalance increases sharply as α increases beyond α_{b} (Fig. 2c).

Noise robustness of balanced and unbalanced solutions

To characterize the effect of noise on the different solutions, we introduce two measures: input-robustness κ_{in} and output robustness κ_{out}, which characterize the robustness of the noise-free solutions to the addition of two types of noise. To ensure robustness to *output* noise, the noise-free membrane potential that is the closest to the threshold must be sufficiently far from it. Thus we define

$$\kappa_{\mathrm{out}} = \min_{\mu} \left| \sum_{i=1}^{N} w_i x_i^{\mu} - 1 \right| \ , \tag{4}$$

9

where the minimum is taken over all the input patterns in the task and the threshold is 1 (because we measure the weights in units of $(V_{\text{th}} - V_{\text{rest}})/\sigma_{\text{exc}}$). The second measure, which characterizes robustness to *input* noise, must take into account the fact that the fluctuations in the membrane potential induced by this form of noise scale with the size of the synaptic weights. Hence, $\kappa_{\text{in}} = \kappa_{\text{out}}/|\boldsymbol{w}|$ (κ_{in} corresponds to the notion of *margin* in machine learning [38]). Efficient algorithms for finding the solution with maximum κ_{in} have been studied extensively [38, 39]. We have developed a novel efficient algorithm for finding solutions with maximum κ_{out} (*SI Methods*).

We now ask what are the possible values of the input and output robustness of unbalanced and balanced solutions. Our theory predicts that the majority of both balanced and unbalanced solutions have vanishingly small values of κ_{in} and κ_{out} and are thus very sensitive to noise. However, for a given load (below capacity) robust solutions do exist, with a spectrum of robustness values up to maximal values, $\kappa_{\text{in}}^{\text{max}} > 0$ and $\kappa_{\text{out}}^{\text{max}} > 0$. Since the magnitude of $\boldsymbol{w}$ scales both signal and noise in the inputs, $\kappa_{\text{in}}^{\text{max}}$ is not sensitive to $|\boldsymbol{w}|$ and hence is of $\mathcal{O}(1)$ for both unbalanced and balanced solutions. On the other hand, $\kappa_{\text{out}}^{\text{max}} = \kappa_{\text{in}}^{\text{max}}|\boldsymbol{w}|$ is proportional to $|\boldsymbol{w}|$. Thus, we expect $\kappa_{\text{out}}^{\text{max}}$ to be of $\mathcal{O}(1)$ when balanced solutions exist and of $\mathcal{O}\left(1/\sqrt{N}\right)$ when only unbalanced solutions exist. In addition, we expect that increasing the load will reduce the value of $\kappa_{\text{in}}^{\text{max}}$ and $\kappa_{\text{out}}^{\text{max}}$ as the number of constraints that need to be satisfied by the synaptic weights increases.

In Fig. 3 we present the values of $\kappa_{\text{in}}^{\text{max}}$ and $\kappa_{\text{out}}^{\text{max}}$ vs. the load. As expected, we find that the value of both $\kappa_{\text{in}}^{\text{max}}$ and $\kappa_{\text{out}}^{\text{max}}$ reach zero as the load approaches the capacity, α_{c} (and diverges, as $N \to \infty$, for vanishingly small loads). However $\kappa_{\text{out}}^{\text{max}}$ is only substantial (of order 1) and proportional to Γ below α_{b} where balanced solutions exist (Fig. 3a-b). In contrast $\kappa_{\text{in}}^{\text{max}}$ remains of order 1 up to the full capacity, α_{c} (Fig. 3c). What are the properties of 'optimal' solutions that achieve the maximal robustness to either input or output noise? We find that the solutions that achieve the maximal output robustness, $\kappa_{\text{out}}^{\text{max}}$, are balanced for all $\alpha \leq \alpha_{\text{b}}$ and their norm saturates the upper bound, Γ (Fig. S3b). Interestingly, for a wide range of input parameters (*SI Methods*, and Fig. S2b), solutions that achieve the maximal input robustness, $\kappa_{\text{in}}^{\text{max}}$, are unbalanced solutions (Fig. S3c). Nevertheless, we find that below the critical balance load, α_{b}, the κ_{in} values of the balanced maximal κ_{out} solutions are of the same order as, and indeed close to, $\kappa_{\text{in}}^{\text{max}}$ (Fig. 3c, dashed gray line). In fact, the balanced solution with maximal κ_{out} also posses the maximal value of κ_{in} that is possible for balanced solutions.

We conclude that solutions that are robust to both input and output noise exist for loads less than α_{b} which for $f_{\text{exc}} > f_{\text{exc}}^{\star}$ is smaller than α_{c} However, as long as f_{exc} is close to $f_{\text{exc}}^{\star}$, the reduction in capacity from α_{c} to α_{b} imposed by the requirement of robustness is small.

Balanced and unbalanced solutions for spiking neurons

Neurons typically receive their input and communicate their output through action potentials. Thus, a fundamental question is how will the introduction of spike-based input and spiking output affect our results. Here we show that the main properties of balanced and unbalanced synaptic efficacies, as discussed above, remain when the inputs are spike trains and the model neuron implements spiking and membrane potential reset mechanisms.
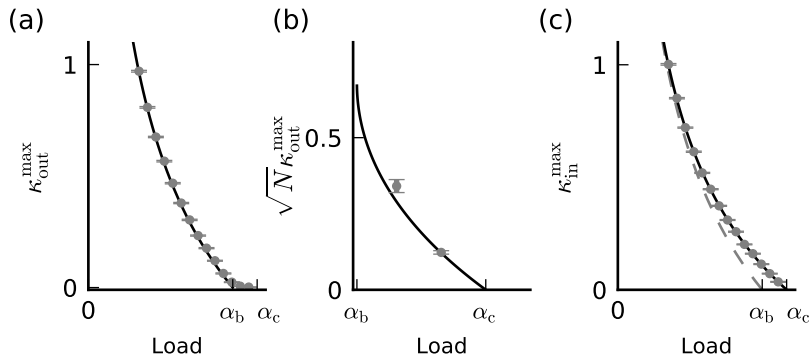
Figure 3: **Maximal values of input and output robustness.** (a) Maximal value of κ_{out} vs. load (in units of $\Gamma\sigma_{\mathrm{exc}}/\left(V_{\mathrm{th}}-V_{\mathrm{rest}}\right)$). No solutions exist above the maximal κ_{out} line ($\kappa_{\mathrm{out}}^{\mathrm{max}}$, black). Below $\kappa_{\mathrm{out}}^{\mathrm{max}}$, for output robustness that is of order 1, only balanced solutions exist. (b) Maximal value of κ_{out} for loads between α_{b} and α_{c} (in units of $\sigma_{\mathrm{exc}}/\bar{x}_{\mathrm{exc}}$). In this range only unbalanced solution exist and the maximal κ_{out} values (black line) scale as $1/\sqrt{N}$. (c) Maximal value of κ_{in} vs. load (in units of σ_{exc}). No solutions exist above the maximal κ_{in} line ($\kappa_{\mathrm{in}}^{\mathrm{max}}$, black). For the parameters used, solutions that achieve $\kappa_{\mathrm{in}}^{\mathrm{max}}$ are unbalanced. The maximal value of κ_{in} for balanced solutions (dashed gray line) is not far from the $\kappa_{\mathrm{in}}^{\mathrm{max}}$ and is attained by solutions that maximize κ_{out} for $\alpha < \alpha_{\mathrm{b}}$. In all panels, theory and numerical results are depicted in black or gray lines and gray dots respectively. Error-bars depict standard error of the mean. See *Methods* for parameters used. For further simulation results see Fig. S3.

We consider a leaky integrate-and-fire (LIF) neuron that is required to perform the same binary classification task we considered using the perceptron. Each input is characterized by a vector of firing rates, $\boldsymbol{x}^\mu$. Each afferent generates a Poisson spike train over an interval from time $t = 0$ to $t = T$, with mean rate $r_i \propto x_i^\mu$. The LIF neuron integrates these input spikes (*Methods*), and emits an output spike whenever its membrane potential crosses a firing threshold. After each output spike, the membrane potential is reset to the resting potential, and the integration of inputs continues. We define the output state of the LIF neuron using the total number of output spikes n_{spikes}: the neuron is quiescent if $n_{\text{spikes}} \leq n_{\text{thr}}$ and active if $n_{\text{spikes}} > n_{\text{thr}}$ were n_{thr} is chosen to maximize classification performance. We will not discuss the properties of learning in LIF neurons [40, 41, 42, 43, 44], but instead test the properties of the solutions (weights) obtained from the perceptron model when they are used for the LIF neuron. In particular, we compare the performance of the balanced, maximal κ_{out} solution and the unbalanced, maximal κ_{in} solution. When the synaptic weight of the LIF neuron are set according to the two perceptron solutions, the mean output of the LIF neuron correctly classifies the input patterns (according to the desired classification; Fig. S4). Consistently with the results for the perceptron, we find that with no output noise the performance of both solutions is good, even in the presence of the substantial input noise caused by Poisson fluctuations in the number of input spikes and their timings (Fig. 4a-c). When the output noise magnitude is increased (*Methods*), however, the performance of the unbalanced maximal κ_{in} solution quickly deteriorates, whereas the performance of the balanced maximal κ_{out} solution remains largely unaffected (Fig. 4d-f). Thus, the spiking model recapitulates the general results found for the perceptron.

Balanced and unbalanced synaptic weights in associative memory networks

Thus far, we have considered the selectivity of a single neuron, but our results also have important implications for recurrently connected neuronal networks, in particular recurrent networks implementing associative memory functions. Models of associative memory in which stable fixed points of the network dynamics represent memories, and memory retrieval corresponds to the dynamic transformation of an initial state to one of the memory-representing fixed points, have been a major focus of memory research for many years [23, 45, 46, 47, 26, 27]. For the network to function as an associative memory, memory states must have large basins of attraction so that the network can perform pattern completion, recalling a memory from an initial state that is similar but not identical to it. In addition, memory retrieval must be robust to output noise. As we will show, the variables κ_{in} and κ_{out} for the synaptic weights projecting onto individual neurons in the network are closely related to the sizes of the basins of attraction of the memories and the robustness to output noise, respectively.

We consider a network that consists of $N f_{\text{exc}}$ excitatory and $N \left(1 - f_{\text{exc}}\right)$ inhibitory, recurrently connected binary neurons. The network operates in discrete time steps and, at each step the state of one randomly chosen neuron, i, is updated according to

$$s_i \left(t + 1\right) = \Theta \left[\sum_{j \neq i} J_{ij} s_j \left(t\right) + \eta_{\text{out}} \left(t\right) - 1\right] . \tag{5}$$

Here $\Theta \left(x\right) = 1$ for $x \geq 0$ and 0 otherwise, J_{ij} is the weight of the synapse from neuron j to neuron i, and $\eta_{\text{out}}(t)$, the output noise, is a Gaussian random variable with standard
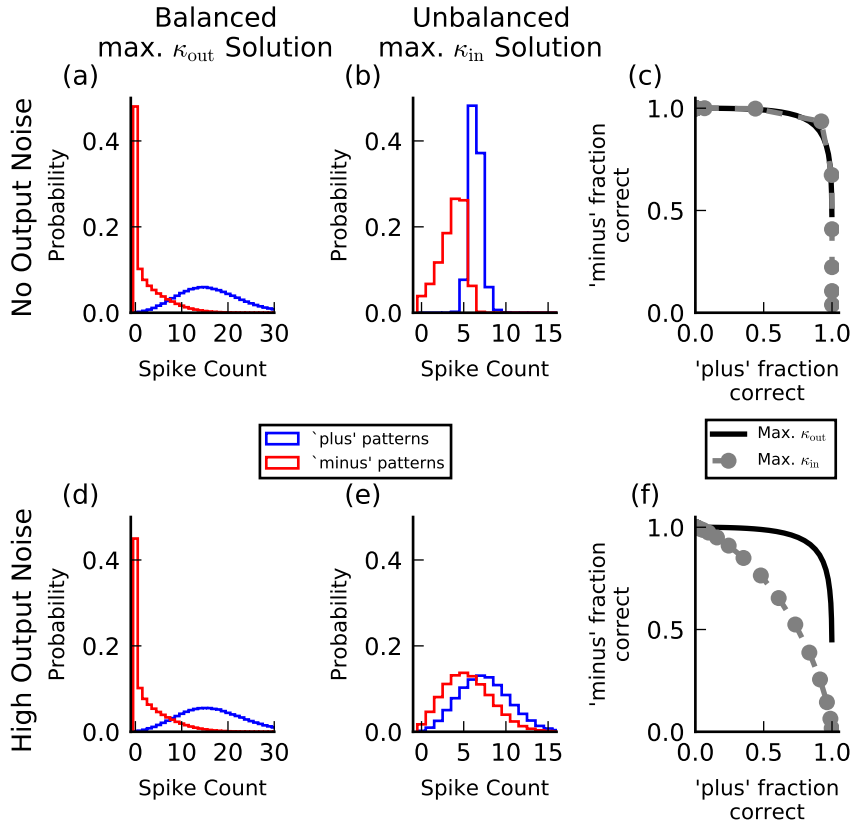
Figure 4: **Selectivity in a spiking model.** Panels (a)-(b) (panels (d)-(e)) depict the output of an LIF neuron with no (high) output noise for the balanced maximal κ_{out} solution ((a) and (d)) and the unbalanced maximal κ_{in} solution ((b) and (e)). Panels (c) and (f) depict the ROC curves for the two solutions under the no output noise (in (c)) and high output noise (in (f)) conditions obtained as the decision threshold (n_{thr}) is modified from 0 to ∞. Consistently with the results of the perceptron, the performance of the two solutions with no output noise is very similar with a slight advantage for the maximal κ_{in} solution. With higher levels of output noise, the performance of the unbalanced maximal κ_{in} solution quickly deteriorates, whereas the performance of the balanced maximal κ_{out} solution is only slightly affected. $|\boldsymbol{w}|$ of the balanced solution was chosen to equalize the mean output spike count across all patterns in both solutions (mean $n_{\mathrm{spike}} \sim 4$). See *Methods* for parameters used.

deviation σ_{out}. P randomly chosen binary activity patterns $\{\mathbf{s}^\mu\}$, $\mu = 1, 2, ..., P$ (where each $s_i^\mu = \{0, 1\}$) representing the stored memories are encoded in the recurrent synaptic matrix J such that they will be fixed points of the network dynamics. This is achieved by treating each neuron, say i, as a perceptron with a weight vector $\boldsymbol{w}^i = \{J_{ij}\}_{j \neq i}$ that maps its inputs $\{s_j^\mu\}$ from all other neurons to its desired output s_i^μ for each memory state (Fig. 5a-b, *Methods*). This creates an attractor network in which the memory states are stable fixed points of the dynamics in the noise-free condition ($\sigma_{\text{out}} = 0$) [19].

The capacity of the memory network is defined as the maximal load for which the memory patterns are stable fixed points of the dynamics. The capacity of a single neuron perceptron depends on the statistics of its desired output (which in our case is the sparsity of activity across memory states). Since this statistic may be different in excitatory and inhibitory populations, the single neuron capacity of the two populations may vary, hence the global capacity of the recurrent network is the minimum of the single-neuron capacities of the two neuron types. As long as P is smaller than this critical capacity, a recurrent weight matrix exists for which all P memory states are stable fixed points of the noiseless dynamics. However such solutions are not unique, and the choice of a particular matrix can endow the network with different robustness properties. As stated above, to properly function as an associative memory the fixed points have large basins of attraction. Corruption of the initial state away from the parent memory pattern introduces variability into the inputs of each neuron for subsequent dynamic iterations and hence is equivalent to injecting input noise in the single-neuron feedforward case. Therefore a large basin of attraction is achieved when the matrix J yields a large input noise robustness for each neuron in the (noise free) fixed points [48, 49]. The requirement that the memory states and retrieval will be robust against output noise is satisfied when J yields a large output noise robustness for each neuron in the (noise free) fixed points. We therefore consider two types of recurrent connections: one in which each row of J is a weight vector that maximizes κ_{in} and hence, in the chosen parameter regime, is necessarily unbalanced; and a second in which the rows of the connection matrix correspond to balanced solutions that maximize κ_{out}.

We estimate the basins of attraction of the memory patterns numerically by initializing the network in states that are corrupted versions of the memory states (*Methods*) and observing if the network, with $\sigma_{\text{out}} = 0$, converges to the parent memory state (Fig. 5c, blue) or diverges away from it (Fig. 5c, red). We define the size of the basin of attraction as the maximum distortion in the initial state that assures convergence to the parent memory with high probability.

Comparing the basins of attraction of the two types of networks, we find that the mean basin of attraction of the unbalanced network is moderately larger than that of the balanced one (Fig. 5d), consistent with the slightly lower value of κ_{in} in the balanced case (Fig. 5d). On the other hand, the behavior of the two networks is strikingly different in the presence of output noise. To illustrate this, we start each network at a memory state and determine if it is stable, (remains in the vicinity of this state for an extended period of time) despite the noise in the dynamics (Fig. 5e). We estimate the output noise tolerance of the network by measuring the maximal value of σ_{out} for which the memory states are stable (Fig. 5f). We find that memory states in the balanced solution with maximal κ_{out} are stable for noise levels that (for the network sizes used in the simulation) are an order of magnitude larger than for the unbalanced network with maximal κ_{in} (Fig. 5f).
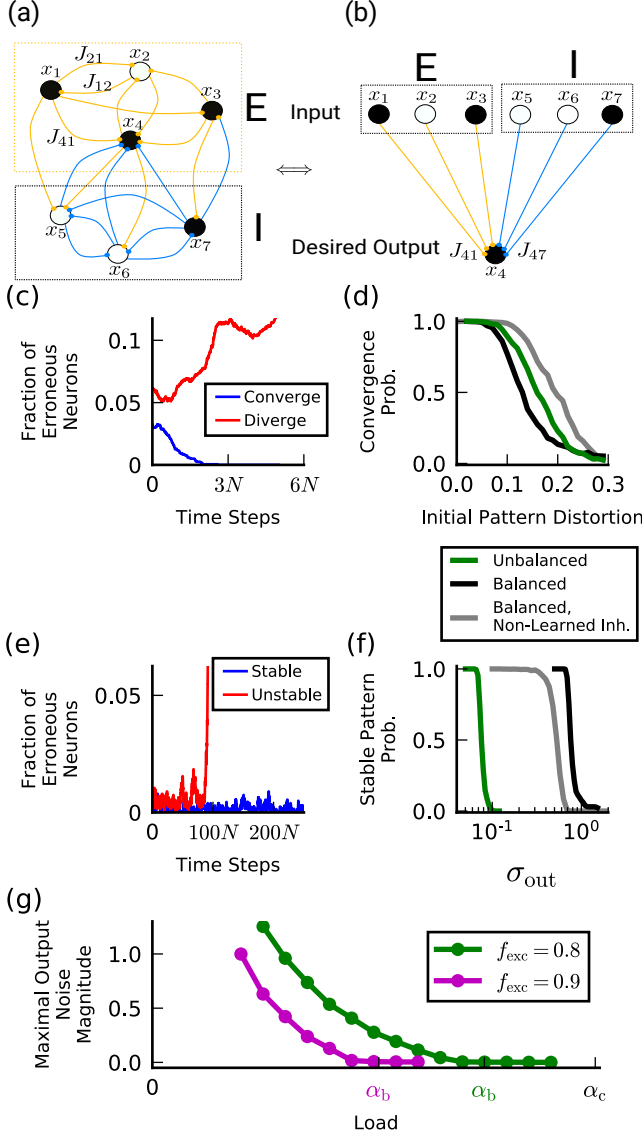
Figure 5: **Recurrent associative memory network constructed using single-neuron feedforward learning.** (a) A fully connected recurrent network of excitatory (E) and inhibitory (I) neurons in a particular memory state. Active (quiescent) neurons are shown in black (white). Excitatory and inhibitory synaptic connections (J_{ij}) are shown in yellow and blue, respectively (not all connections are depicted). Lines symbolize axons, and synapses are shown as small circles. (b) To find an appropriate J_{ij}, the postsynaptic weights of each neuron are set using the memory-state activities of the other neurons as input and its own memory state as the desired output. In this example, neuron #4 will implement its desire memory state through modification of the weights J_{4j} for $j = 1, 2, 3, 5, 6, 7$. (c) and (e) show the fraction of erroneous (different from a given memory pattern) neurons in the network as a function of time. (c) Network dynamics with $\sigma_{\text{out}} = 0$. An initial state of the network can either converge to the memory state (blue) or diverge to other network states (red). (d) Probability of converging to a memory state steps vs. initial pattern distortion (*Methods*) for a network with unbalanced maximal κ_{in} weights (green), a network with balanced maximal κ_{out} weights (black) and a network with balanced maximal κ_{out} weights with unlearned inhibition (gray, see text). (e) Network dynamics with $\sigma_{\text{out}} > 0$. The network is initialized at the memory state. The dynamics can be stable (blue; the network remains close to the memory state), or unstable (red; the network diverge to another state). (f) Probability of stable dynamics for at least $500N$ time steps for networks initialized at the memory state in the presence of output noise vs. σ_{out}. Colors are the same as in (d). (g) Maximal output noise magnitude vs. load for networks with balanced synaptic weights matrix maximizing κ_{out}. Similarly to κ_{out}, the maximal output noise magnitude is of order 1 only below α_{b}. Above it, even though solutions exists they are extremely sensitive to output noise. Results are shown for $f_{\text{exc}} = 0.8$ (green) and $f_{\text{exc}} = 0.9$ (magenta). See *Methods* for parameters used.

Finally, we ask how the noise robustness of the memory states in the balanced network depends on the number of memories. As shown in Fig. 5f, for a fixed level of load below capacity, memory patterns are stable ($P_{\text{stable}} > 0.5$) as long as levels of noise remain below a threshold value, which we denote as $\sigma_{\text{out}}^{\max}(\alpha)$. When σ_{out} increases beyond $\sigma_{\text{out}}^{\max}(\alpha)$ stability of the memory states rapidly deteriorates. The critical noise function $\sigma_{\text{out}}^{\max}(\alpha)$ decreases smoothly from a large value at small α to zero at a level of load, α_{b}. This load coincides with the maximal load for which both excitatory and inhibitory neurons have balanced solution (Fig. 5g). For loads $\alpha_{\text{b}} < \alpha < \alpha_{\text{c}}$, all solutions are unbalanced, hence the magnitude of the stochastic dynamical component can be at most of order $1/\sqrt{N}$.

The role of inhibition in associative memory networks

In our associative memory network model, we assumed that both excitatory and inhibitory neurons code desired memory states and that all network connections are modified by learning. Most previous models of associative memory that separate excitation and inhibition assume that memory patterns are restricted to the excitatory population, whereas inhibition provides stabilizing inputs [50, 51, 52, 53, 14, 47]. To address the emergence of balanced solution in scenarios where the inhibitory neurons do not represent long-term memories, we studied an architecture where I to E, I to I and E to I connections are random sparse matrices with large amplitudes, resulting in inhibitory activity patterns driven by the excitatory memory states. In such conditions, the inhibitory subnetwork exhibits irregular asynchronous activity with an overall mean activity that is proportional to the mean activity of the driving excitatory population [7, 54, 55]. Although the mean inhibitory feedback provided to the excitatory neurons can balance the mean excitation, the variability in this feedback injects substantial noise onto the excitatory neurons, which degrades system performance (*SI Methods*). This variability stems from the differences in inhibitory activity patterns generated by the different excitatory memory states (albeit with the same mean). Additional noise is caused by the temporal irregular activity of the chaotic inhibitory dynamics. Next we ask whether system's performance can be improved through plasticity in the I to E connections for which some experimental evidence exist [56, 57, 22, 58, 59]. Indeed, we find an appropriate plasticity rule for this pathway (*SI Methods*) that suppresses the spatio-temporal fluctuations in the inhibitory feedback, yielding a balanced state that behaves similarly to the fully learned networks described above (Fig. 5d, 5f, gray lines). Interestingly, in this case the basins of attraction of the balanced network are comparable to or even larger than the basins of the unbalanced fully learned network (compared gray to green curves in Fig. 5d). Despite the fact that no explicit memory patterns are assigned to the the inhibitory populations, the inhibitory activity plays a computational role that goes beyond providing global inhibitory feedback; when the weights of the I to E connections are shuffled, the network's performance significantly degrades (Fig. S5).

Learning Robust Solutions

Thus far, we have presented analytical and numerical investigations of solutions that support selectivity or associative memory and provide substantial robustness to noise. However, we did not address the way in which these robust solutions could be learned by a biological system.

16

In fact, as stated above, the majority of solutions for these tasks have vanishingly small output and input robustness. Therefore, an important question is whether noise robust weights can emerge naturally from synaptic learning rules that are appropriate for neuronal circuits.

The actual algorithms used for learning in the neural circuits are generally unknown, especially within a supervised learning scenario. Experiments suggest that learning rules may depend on brain area and both pre and post synaptic neuron types (see for example [60, 56, 57, 58], for reviews see [59, 61, 62, 63]). Regardless of the particular learning algorithm used, however, our theory suggests that a simple way to ensure that learning arrives at a robust solution is to introduce noise during learning. Indeed, this is a common practice in machine learning for increasing generalization abilities (a specific form of *data augmentation*, [64, 65]). The rationale is that learning algorithms that achieve low error in the presence of noise necessarily lead to solutions that are robust against noise levels at least as large as those present during learning. In the case we are considering, learning in the presence of substantial *input noise* should lead to solutions that have substantial κ_{in} and introducing *output noise* during learning should lead to solutions with substantial κ_{out}. We note that κ_{in} may be large even if κ_{out} remains small (for example, in unbalanced solutions with maximal κ_{in}) but not *vice versa* (because κ_{out} of order 1 implies $|\boldsymbol{w}|$ (and as a result κ_{in}) of order 1 as well). Therefore, learning in the presence of significant output noise should lead to solutions that are robust to both input and output noise, whereas learning in the presence of input noise alone may lead to unbalanced solutions that are sensitive to output noise, depending on details of the learning algorithm. We therefore predict that performing successful learning in the presence of output noise is a sufficient condition for the emergence of excitation-inhibition balance.

To demonstrate that robust balanced solutions emerge in the presence of output noise, we consider a variant of the perceptron learning algorithm [17] in which we have forced the sign constraints on the weights [28] and, in addition, added a weight decay term implementing a soft constraint on the magnitude of the weights (*Methods*). This supervised learning rule possesses several important properties that are required for biological plausibility: It is on-line, weights are modified incrementally after each pattern presentation; It is history independent so that each weight update only depends on the current pattern and error signal; Lastly, it is simple and local, weight updates are a function of the error signal and quantities that are available locally at the synapse (presynaptic activity and synaptic efficacy). When this learning rule is applied to train a selectivity task in the presence of substantial output noise, the resulting solution has a balanced weight vector with substantial κ_{out} and κ_{in} (Fig. S6, black). In contrast, if learning occurs with weak output noise, the resulting solution is unbalanced with small κ_{out}, while its κ_{in} may be large if substantial input noise is present during learning (Fig. S6, gray). When this learning rule is applied in the load regime where only unbalanced solutions exist ($\alpha_{\text{b}} < \alpha < \alpha_{\text{c}}$), learning fails to achieve reasonable performance when applied in the presence of large output noise. When noise is scaled down to the value allowed by $\kappa_{\text{out}}^{\max} \propto 1/\sqrt{N}$, learning yields unbalanced solutions with robustness values of the order of the maximum allowed in this region (Fig. S6).

Figure 6: **Emergence of E-I balance from learning in the presence of output noise.** All panels show the outcome of perceptron learning for a noisy neuron (*Methods*) under low ($\sigma_{\text{out}} = 0.01$, gray) and high output noise conditions ($\sigma_{\text{out}} = 0.1$, black). Except for σ_{out}, all model and learning parameters are identical for the two conditions (including $\sigma_{\text{in}} = 0.1$). (a) Mean training error vs. learning cycle. On each cycle, all the input patterns to be learned are presented once. The error decays and plateaus at its minimal value under both low and high output noise conditions (b) Mean imbalance index (IB, eq. 3) vs. learning cycle. IB remains of order 1 under low output noise conditions and drops close to zero under high output noise conditions. (c) Mean input robustness (κ_{in}) vs. learning cycle. Input robustness is high under both output noise

conditions. (d) Mean output robustness (κ_{out}) vs. learning cycle. Output robustness is substantial only under the high output noise learning condition. These results demonstrate that robust balanced solutions naturally emerge under learning in the presence of high output noise. See *Methods* for other parameters used.
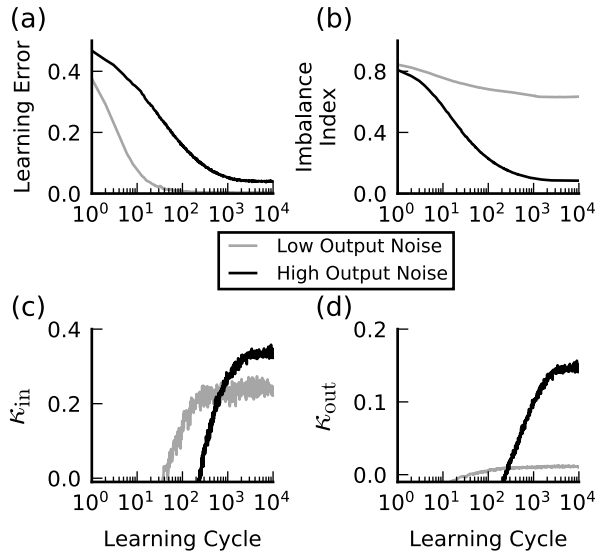
Discussion

The results we have presented come from imposing a set of fundamental biological constraints: fixed-sign synaptic weights, non-negative afferent activities, a positive firing threshold (relative to the resting potential), and both input and output forms of noise. Amit et al. [22] studied the maximal margin solution for the sign-constrained perceptron and showed that it has half the capacity of the unconstrained perceptron. However, this previous work considered afferent activities that were centered around zero and a neuron with zero firing threshold, features that preclude the presence of the novel behavior exhibited by the more biologically constrained model studied here. Chapeton et al. [26] studied perceptron learning with sign-constrained weights and a preassigned level of robustness, but only considered solutions in the unbalanced regime which, as we have shown, are extremely sensitive to output noise.

Learning in neural circuits involves a trade-off between exhausting the system's capacity for implementing complex input-output functions on the one hand, and ensuring good generalization properties on the other. A well-known approach in machine learning has been to search for solutions that fit the training examples while maximizing the distance of samples from the decision surface, a strategy known as maximizing the margin [38, 20, 22]. The margin being maximized in this case corresponds, in our framework, to κ_{in}. Work in computational neuroscience has implicitly optimized a robustness parameter equivalent to our κ_{out} [24, 26]. To our knowledge, the two approaches have not been distinguished before nor shown to result in solutions with dramatically different noise sensitivities. In particular, over a wide param-

eter range, we have shown that maximizing κ_{out} leads to a balanced solution with minimal sensitivity to output noise and robustness to input noise that is almost as good as that of the maximal margin solution, with only a modest trade-off in capacity. On the other hand, maximizing the margin (κ_{in}) often leads to unbalanced solutions with extreme sensitivity to output noise.

The perceptron has long been considered a model of cerebellar learning and computation [66, 67]. More recently, Brunel et al. [24] investigated the capacity and robustness of a perceptron model of a cerebellar Purkinje cell, taking all weights to be excitatory. In view of the analysis presented here, balanced solutions are not possible in this case ($f_{\text{exc}} = 1$), and solutions that maximize either input-noise or output-noise robustness both have $\kappa_{\text{out}} \propto 1/\sqrt{N}$. These two types of solutions differ in their weight distributions, with experimentally testable consequences for the predicted circuit structure (*SI Methods* and Fig. S2c; Brunel et al. [24] only considered solutions that maximize κ_{out}). Output robustness of the unbalanced solutions can be increased by making the input activity patterns sparse. Denoting by s the mean fraction of active neurons in the input, maximum output robustness scales as $\kappa_{\text{out}} \sim 1/\sqrt{Ns}$ (Fig. 3b, and *SI Methods*). Thus, the high sparsity in input activation (granule cell activity) of the cerebellum relative to the modest sparsity in the neocortex is consistent with the former being dominated by excitatory modifiable synapses.

Interestingly, our results suggests an optimal ratio of excitatory to inhibitory synapses. Capacity in the balanced regime is optimal when $f_{\text{exc}} = f_{\text{exc}}^{\star}$, with $f_{\text{exc}}^{\star}$ determined by the coefficients of variation (with respect to stimulus) of the excitatory and inhibitory inputs (eq. 2). Thus, optimality predicts a simple relation between the fraction of excitatory and inhibitory inputs and their degree of tuning. Estimating the CV's from existing data is difficult, but it would be interesting to check if input statistics and connectivity ratios in different brain areas are consistent with this prediction. The commonly observed value in cortex, $f_{\text{exc}} \simeq 0.8$, would be optimal for input statistics with $\text{CV}_{\text{exc}}/\text{CV}_{\text{inh}} \simeq 4$. In general, we expect that $\text{CV}_{\text{exc}}/\text{CV}_{\text{inh}} > 1$ which implies that $f_{\text{exc}}^{\star} > 1/2$.

For most of our work, we assumed that inhibitory neurons learn to represent specific sensory and long-term memory information, just as the excitatory ones and that all synaptic pathways are learned using similar learning rules. While plasticity in both excitatory and inhibitory pathways have been observed [60, 56, 57, 58, 62, 63, 68], accumulating experimental evidence indicates a high degree of cell type and synaptic type specificity of the plasticity rules. In addition, synaptic plasticity is under tight control of neuromodulatory systems. At present, it is unclear how to interpret our learning rules in terms of concrete experimentally observed synaptic plasticity. Other functional models of neural learning assume learning only within excitatory population with inhibition acting as global stabilizing force. In the case of sensory processing, our approach is consistent with the observation of a similar stimulus tuning of EPSCs and IPSCs in many cortical sensory areas. The role of inhibitory neurons in memory representations is less known (but see [69]). Importantly, we have shown that our main results are valid also in the case in which inhibitory neurons do not explicitly participate in the coding of the memories. Interestingly, our work suggests that even if inhibitory neurons are only passive observers during learning processes, learning of inhibitory synapses onto excitatory cells can amplify the memory stability of the system against fluctuations in the inhibitory feedback. Given the diversity of inhibitory cell types it is likely that in the real circuits inhibition plays multiple roles, including both conveying information and providing stability.

Several previous models of associative memory have incorporated biological constraints on the sign of the synapses, Dale's Law, assuming variants of Hebbian plasticity in the E to E synapses [50, 51, 53, 52, 14, 47]. The capacity of the these Hebbian models is relatively poor, and their basins of attractions small, except at extremely sparse activity levels. In contrast, our model applies a more powerful learning rule that, while keeping the sign constraints on the synapses, exhibits significantly superior performance: with high capacity even for moderate sparsity levels, large basins of attraction and high robustness to output noise.

From a dynamical systems perspective, the associative memory networks we construct exhibit unusual properties. In most associative memory network models large basins of attractions endow the memory state with robustness against stochasticity in the dynamics (*i.e.*, output noise). Here, we found that, for the same set of fixed-point memories, the synaptic weights with the largest possible basins (the unbalanced solutions with maximal κ_{in}) are very sensitive to even mild levels of stochasticity, whereas the balanced synaptic weights with somewhat reduced basins have substantially increased output noise robustness.

At the network level, as at the single-neuron level, imposing basic features of neural circuitry – positive inputs, bounded synapses of fixed sign, a positive firing threshold, and sources of noise – force neural circuits into the balanced regime. A recent class of models showing computational benefits of balanced inputs use extremely strong synapses, which are outside the range we have discussed [16]. These models are stabilized by instantaneous transmission of signals between neurons which are not required in the range of synaptic strength we consider.

Previous models of balanced networks have highlighted the ability of network with strong excitatory and inhibitory recurrent synapses to settle into a state in which the total input is dynamically balanced without special tuning of the synaptic strengths. Such a state is characterized by a high degree of intrinsically generated spatio-temporal variability [7]. Mean population activities respond fast and in a linear fashion to external inputs. Typically, these networks lack the population level nonlinearity required to generate multiple attractors. In contrast, we have explored the capacity of balanced network to support multiple stable fixed-points by tuning the synaptic strengths through appropriate learning. Despite the dynamic and functional differences in the two classes of networks, the balancing of excitation and inhibition plays a similar role in both. In the first scenario, synaptic balance amplifies small changes in the spatial or temporal properties of the external drive. Similarly, in the present scenario, balanced synaptic architecture leads to enhanced robustness by amplifying the small variations in the synaptic inputs induced by changes in the stimulus or memory identity. It would be interesting to combine fast dynamics with robust associative memory capabilities.

In conclusion, we have uncovered a fundamental principle of neuronal learning under basic biological constraints. Our work reveals that excitation-inhibition balance may have a critical computational role in producing robust neuronal functionality that is insensitive to output noise. We showed that this balance is important at the single neuron level for both spiking and non-spiking neurons, and at the level of recurrently connected neural networks. Further, the theory suggests that excitation-inhibition balance may be a collective, self-maintaining, emergent phenomena of synaptic plasticity. Any successful neuronal learning process in the presence of substantial output noise will lead to strong balanced synaptic efficacies with noise robustness features. The fundamental nature of this result suggests that it should apply across a variety of neuronal circuits that learn in the presence of noise.

Methods

Finding perceptron solutions

There are a number of numerical methods for choosing a weight vector $\boldsymbol{w}$ that generates a specified selectivity [28, 24, 26, 38]. For numerical simulations we developed algorithms that find the maximal κ_{out} and maximal κ_{in} solutions that obey the imposed biological constraints. These solutions can be found directly by solving conic programing optimization problems for which efficient algorithms exist and are widely available [70]. For details see *SI Methods*.

Simulations of recurrent networks

Memory states: Networks were trained to implement a set of P memory states, specified by $x_i^\mu \in \{0, 1\}$, $i = 1, 2, \ldots, N$, $\mu = 1, 2, \ldots, P$, as stable fixed points of the noise free dynamics. Memory states were randomly chosen i.i.d. from binary distributions with parameter $p_{\text{exc/inh}}$ according to the type of the i'th input afferent, *i.e.*, $\Pr(x_i^\mu = 1) = p_{\text{exc/inh}}$ and $\Pr(x_i^\mu = 0) = 1 - p_{\text{exc/inh}}$. **Initial pattern distortion:** To start the network close to a memory state $\boldsymbol{x}^\mu$, the initial state of the network, $s_i\,(t = 0)$ for $i = 1, 2, \ldots, N$, was randomly chosen according to $\Pr(s_i = 1) = (1 - \delta)\,\Theta\,(2x_i^\mu - 1) + \delta\frac{p_{\text{exc/inh}}}{1 - p_{\text{exc/inh}}}\Theta\,(-2x_i^\mu + 1)$ where δ is the initial pattern distortion level (Fig. 5b) and $\Theta\,(x) = 1$ for $x \geq 0$ and 0 otherwise. This procedure ensures that the mean activity levels of excitatory and inhibitory neurons in the initial state is the same as the their mean activity levels in the memory state [71].

Perceptron learning algorithm

The perceptron learning algorithm learns to classify a set of P labeled patterns. At learning time step t one pattern $\boldsymbol{x}_t$ with desired output $y_t = \pm 1$ is presented to the neuron. The output of the perceptron s_t is given by $s_t = \text{sign}\left(\boldsymbol{w}_t^{\text{T}}\boldsymbol{x}_t + \eta_t - 1\right)$, where η_t is a Gaussian random variable with zero mean and variance $|\boldsymbol{w}_t|^2\,\sigma_{\text{in}}^2 + \sigma_{\text{out}}^2$. The error signal is defined as $e_t = y_t\Theta\,(-s_ty_t)$ where $\Theta\,(x) = 1$ for $x > 0$ and zero otherwise. After each pattern presentation all synapses are updated. The synaptic weights of excitatory inputs are updated according to $w_{i,t+1} = \left[(1 - \varepsilon)\,w_{i,t} + \rho e_t x_{i,t}\right]_+$ and weights of inhibitory inputs are updated according to $w_{i,t+1} = \left[(1 - \varepsilon)\,w_{i,t} + \rho e_t x_{i,t}\right]_-$ where $[x]_\pm = x\Theta\,(\pm x)$, ε is a weight decay constant and ρ is a constant learning rate. At each learning cycle (P learning time steps) all patterns are presented sequentially in a random order (randomized at each learning cycle).

Random patterns in numerical estimation of $\kappa_{\text{out}}^{\text{max}}$ and $\kappa_{\text{in}}^{\text{max}}$ solutions

In numerical experiments for Fig. 3, Fig. 4, Fig. S1 and Fig. S3, excitatory inputs for the random patterns were drawn i.i.d from an exponential distribution with unity mean and standard deviation. Inhibitory inputs were drawn from a Gamma distribution with shape parameter k and scale parameter θ (The PDF of the Gamma distribution is given by $P\,(x) = \frac{1}{\Gamma(k)\theta}\left(\frac{x}{\theta}\right)^{k-1}e^{-\frac{x}{\theta}}$ where $\Gamma\,(k)$ is the Gamma function).

Dynamics of Leaky Integrate-and-Fire neuron

Input spike-trains: For each input pattern $\boldsymbol{x}^\mu$ input spike trains of input afferent $i = 1, 2, ..., N$ were drawn randomly from a Poisson processes with rate $r_i = Ax_i^\mu$, for duration T. **Synaptic Input:** Given the set of input spike trains $\{t_i\}$, $i = 1, 2, ..., N$ the contribution of synaptic input to the membrane potential is given by $V_{\mathrm{syn}}(t) = \sum_i w_i \sum_{t_i} K(t - t_i)$ where w_i is the synaptic efficacy of the synapse from the i'th input afferent and $K(t)$ is a post synaptic potential kernel. $K(t) = 0$ for $t < 0$ and is given by $K(t) = V_0 \left(e^{-\frac{t}{\tau_{\mathrm{m}}}} - e^{-\frac{t}{\tau_{\mathrm{s}}}} \right)$ for $t > 0$ where τ_{m} and τ_{s} are the membrane and synaptic time constants respectively, and V_0 is such that the maximal value of $K(t)$ is one **Output noise:** Output noise was added to the neuron's membrane potential as random synaptic input $V_{\mathrm{o.n.}}(t) = \sum_{j=1}^{N_{\mathrm{noise}}} g_j K(t - t_j)$ were g_j was randomly drawn from a zero mean Gaussian distribution with standard deviation σ_{n} and $t_j \in (0, T)$ was randomly drawn from a uniform distribution. **Voltage reset:** After each threshold crossing the membrane potential was reset to it's resting potential. Given the set of output spike times $\{t_{\mathrm{spike}}\}$, the total contribution of voltage reset to the membrane potential can be written as $V_{\mathrm{reset}}(t) = -(V_{\mathrm{th}} - V_{\mathrm{rest}}) \sum_{t_{\mathrm{spike}}} R(t - t_{\mathrm{spike}})$ where V_{rest} and V_{th} are the neuron's resting and threshold potential respectively and $R(t)$ implements the post-spike voltage reset. $R(t) = 0$ for $t < 0$ and is given by $R(t) = e^{-\frac{t}{\tau_{\mathrm{m}}}}$ for $t \geq 0$. This form ensures the voltage is reset to the resting potential immediately after an output spike. **Membrane potential:** Finally, the neuron's membrane potential is given by $V(t) = V_{\mathrm{rest}} + V_{\mathrm{syn}}(t) + V_{\mathrm{o.n.}}(t) + V_{\mathrm{reset}}(t)$ where V_{reset} is computed given V_{syn} and $V_{\mathrm{o.n.}}$.

Figures parameters

Fig. 2: In all panels $\sigma_{\mathrm{inh}}/\sigma_{\mathrm{exc}} = 2$ and $\mathrm{CV}_{\mathrm{exc}}/\mathrm{CV}_{\mathrm{inh}} = \sqrt{2}$. $\sigma_{\mathrm{inh}}/\sigma_{\mathrm{exc}} = 2$, $\mathrm{CV}_{\mathrm{exc}}/\mathrm{CV}_{\mathrm{inh}} = \sqrt{2}$ with an even split between responsive/unresponsive labels. In (b) and (c) $f_{\mathrm{exc}} = 0.8$. **Fig. 3:** In all panels $N = 3000$, $k = 2$ and $\theta = \sqrt{2}$ leading to $\sigma_{\mathrm{inh}}/\sigma_{\mathrm{exc}} = 2$ $\mathrm{CV}_{\mathrm{exc}}/\mathrm{CV}_{\mathrm{inh}} = \sqrt{2}$, $f_{\mathrm{exc}} = 0.8$ with an even split between responsive/unresponsive labels. Numerical results are averaged over 100 samples. **Fig. 4:** In all panels $N = 1000$, $P = 1000$, fraction of 'plus' patterns $p_{\mathrm{out}} = 0.1$, $f_{\mathrm{exc}} = 0.8$, $V_{\mathrm{rest}} = 0$, $V_{\mathrm{thr}} = 1$, $\tau_{\mathrm{m}} = 30\mathrm{msec}$, $\tau_{\mathrm{s}} = 10\mathrm{msec}$, $T = 200\mathrm{msec}$, $A = 30\mathrm{Hz}$. Random patterns were drawn as described above with $k = 2$ and $\theta = \sqrt{2}$. Maximal κ_{out} solutions were found with $\Gamma = 1.5$ in units of $(V_{\mathrm{th}} - V_{\mathrm{rest}})/\sigma_{\mathrm{exc}}$. No output noise was added in panels (a)-(c). In panels (d)-(e) output noise was added with $N_{\mathrm{noise}} = 30,000$ and $\sigma_{\mathrm{n}} = 2/\sqrt{N_{\mathrm{noise}}}$ (see above). **Fig. 5:** In panels (c)-(f) $N = 2000$, $P = 1000$, $f_{\mathrm{exc}} = 0.8$, $p_{\mathrm{exc}} = 0.1$, $p_{\mathrm{inh}} = 0.2$, $\Gamma = 10\sqrt{p_{\mathrm{exc}}(1 - p_{\mathrm{exc}})}$ in units of $(V_{\mathrm{th}} - V_{\mathrm{rest}})/\sigma_{\mathrm{exc}}$. In (d) and (f) results are averaged over 10 networks and 10 patterns from each network. See *SI Methods* for parameters of inhibitory connectivity of the non learned inhibition networks (gray lines). In panel (g) maximal output noise magnitude is defined as the value of σ_{out} for which the stable pattern probability is $1/2$. To minimize finite size effects in simulations we used $N = 3000$, $f_{\mathrm{exc}} = 0.8$, $p_{\mathrm{exc}} = 0.5$, $p_{\mathrm{inh}} = 0.5$, $\Gamma = 10\sqrt{p_{\mathrm{exc}}(1 - p_{\mathrm{exc}})}$ in units of $(V_{\mathrm{th}} - V_{\mathrm{rest}})/\sigma_{\mathrm{exc}}$. Stable pattern probability for each load and noise level was estimated by averaging over 5 networks and 20 patterns from each network. **Fig. S6:** Random patterns are binary pattern $x_i^\mu \in \{0, 1\}$ with equal probabilities and an even split of 'plus' and 'minus' patterns. $N = 3000$, $P = 900$. Learning algorithm parameters: $\varepsilon = 5 \cdot 10^{-7}$, $\rho = 0.1/N$, $\sigma_{\mathrm{in}} = 0.1$. Results are averaged over 50 samples.

Software

To acknowledge their contribution to scientific work we cite the open source projects that directly and most crucially contributed to the current work. All computational aspects of this work were done using the Python stack of scientific computing (CPython, Numpy, Scipy, Matplotlib [72], Jupyter/Ipython [73] and others). Convex conic optimization was performed using CVXOPT [70]. Parallelization of simulations on a cluster computer was performed using IPyparallel.

Code availability

Python code for simulations and numerical solution of saddle point equations is available upon request.

Acknowledgments

References

[1] Anderson JS, Carandini M, Ferster D (2000) Orientation Tuning of Input Conductance, Excitation, and Inhibition in Cat Primary Visual Cortex. *Journal of Neurophysiology* 84(2):909–926.

[2] Wehr M, Zador AM (2003) Balanced inhibition underlies tuning and sharpens spike timing in auditory cortex. *Nature* 426(6965):442–446.

[3] Okun M, Lampl I (2008) Instantaneous correlation of excitation and inhibition during ongoing and sensory-evoked activities. *Nature Neuroscience* 11(5):535–537.

[4] Poo C, Isaacson JS (2009) Odor representations in olfactory cortex: "sparse" coding, global inhibition, and oscillations. *Neuron* 62(6):850–861.

[5] Atallah BV, Scanziani M (2009) Instantaneous Modulation of Gamma Oscillation Frequency by Balancing Excitation with Inhibition. *Neuron* 62(4):566–577.

[6] Isaacson JS, Scanziani M (2011) How Inhibition Shapes Cortical Activity. *Neuron* 72(2):231–243.

[7] van Vreeswijk C, Sompolinsky H (1996) Chaos in neuronal networks with balanced excitatory and inhibitory activity. *Science* 274(5293):1724–1726.

[8] Vreeswijk Cv, Sompolinsky H (1998) Chaotic Balanced State in a Model of Cortical Circuits. *Neural Computation* 10(6):1321–1371.

[9] Froemke RC, Merzenich MM, Schreiner CE (2007) A synaptic memory trace for cortical receptive field plasticity. *Nature* 450(7168).

[10] Dorrn AL, Yuan K, Barker AJ, Schreiner CE, Froemke RC (2010) Developmental sensory experience balances cortical excitation and inhibition. *Nature* 465(7300):932–936.

[11] Sun YJ et al. (2010) Fine-tuning of pre-balanced excitation and inhibition during auditory cortical development. *Nature* 465(7300):927–931.

[12] Li Yt, Ma Wp, Pan Cj, Zhang LI, Tao HW (2012) Broadening of Cortical Inhibition Mediates Developmental Sharpening of Orientation Selectivity. *Journal of Neuroscience* 32(12):3981–3991.

[13] Tsodyks MV, Sejnowski T (1995) Rapid state switching in balanced cortical network models. *Network: Computation in Neural Systems* 6(2):111–124.

[14] van Vreeswijk C, Sompolinsky H (2005) Course 9 - Irregular Activity in Large Networks of Neurons in *Les Houches*, Methods and Models in Neurophysics, eds. C.C. C, B. G, D. H, C. M, J. D. (Elsevier) Vol. 80, pp. 341–406. DOI: 10.1016/S0924-8099(05)80015-0.

[15] Lim S, Goldman MS (2013) Balanced cortical microcircuitry for maintaining information in working memory. *Nature Neuroscience* 16(9):1306–1314.

[16] Boerlin M, Machens CK, Denève S (2013) Predictive Coding of Dynamical Variables in Balanced Spiking Networks. *PLOS Comput Biol* 9(11):e1003258.

[17] Rosenblatt F (1962) *Principles of neurodynamics: Perceptrons and the theory of brain mechanisms.* (Spartan Books, Washington, DC).

[18] Minsky ML, Papert SA (1988) *Perceptrons: expanded edition.* (MIT Press Cambridge, MA, USA).

[19] Gardner E (1987) Maximum storage capacity in neural networks. *Europhys. Lett.* 4(4):481–485.

[20] Gardner E (1988) The space of interactions in neural network models. *Journal of Physics A: Mathematical and General* 21(1):257.

[21] Gardner E, Derrida B (1988) Optimal storage properties of neural network models. *J. Phys. A: Math. Gen* 21(1):271–284.

[22] Amit DJ, Campbell C, Wong KYM (1989) The interaction space of neural networks with sign-constrained synapses. *Journal of Physics A: Mathematical and General* 22:4687.

[23] Hopfield JJ (1982) Neural networks and physical systems with emergent collective computational abilities. *Proceedings of the National Academy of Sciences* 79(8):2554–2558.

[24] Brunel N, Hakim V, Isope P, Nadal JP, Barbour B (2004) Optimal Information Storage and the Distribution of Synaptic Weights: Perceptron versus Purkinje Cell. *Neuron* 43(5):745–757.

[25] Clopath C, Nadal JP, Brunel N (2012) Storage of Correlated Patterns in Standard and Bistable Purkinje Cell Models. *PLOS Computational Biology* 8(4):e1002448.

[26] Chapeton J, Fares T, LaSota D, Stepanyants A (2012) Efficient associative memory storage in cortical circuits of inhibitory and excitatory neurons. *Proceedings of the National Academy of Sciences* 109(51):E3614–E3622.

[27] Brunel N (2016) Is cortical connectivity optimized for storing information? *Nature Neuroscience* 19(5):749–755.

[28] Amit DJ, Wong KYM, Campbell C (1989) Perceptron learning with sign-constrained weights. *Journal of Physics A: Mathematical and General* 22(12):2039.

[29] Denève S, Machens CK (2016) Efficient codes and balanced networks. *Nature Neuroscience* 19(3):375–382.

[30] Brown DA, Adams PR (1980) Muscarinic suppression of a novel voltage-sensitive K+ current in a vertebrate neurone. *Nature* 283(5748):673–676.

[31] Madison DV, Nicoll RA (1984) Control of the repetitive discharge of rat CA 1 pyramidal neurones in vitro. *The Journal of Physiology* 354:319–331.

[32] Fleidervish IA, Friedman A, Gutnick MJ (1996) Slow inactivation of Na+ current and slow cumulative spike adaptation in mouse and guinea-pig neocortical neurones in slices. *The Journal of Physiology* 493(1):83–97.

[33] Benda J, Herz AVM (2003) A Universal Model for Spike-Frequency Adaptation. *Neural Computation* 15(11):2523–2564.

[34] Cover TM (1965) Geometrical and Statistical Properties of Systems of Linear Inequalities with Applications in Pattern Recognition. *IEEE Transactions on Electronic Computers* EC-14(3):326–334.

[35] Venkatesh SS (1986) Epsilon capacity of neural networks in *AIP Conference Proceedings*. (AIP Publishing), Vol. 151, pp. 440–445.

[36] Liu Bh et al. (2009) Visual Receptive Field Structure of Cortical Inhibitory Neurons Revealed by Two-Photon Imaging Guided Recording. *Journal of Neuroscience* 29(34):10520–10532.

[37] Kerlin AM, Andermann ML, Berezovskii VK, Reid RC (2010) Broadly Tuned Response Properties of Diverse Inhibitory Neuron Subtypes in Mouse Visual Cortex. *Neuron* 67(5):858–871.

[38] Vapnik V (2000) *The nature of statistical learning theory.* (springer).

[39] Bottou L, Lin CJ (2007) Support vector machine solvers. *Large scale kernel machines* pp. 301–320.

[40] Gütig R, Sompolinsky H (2006) The tempotron: a neuron that learns spike timing–based decisions. *Nature Neuroscience* 9(3):420–428.

[41] Memmesheimer RM, Rubin R, Ölveczky BP, Sompolinsky H (2014) Learning Precisely Timed Spikes. *Neuron* 82(4):925–938.

[42] Gütig R (2016) Spiking neurons can discover predictive features by aggregate-label learning. *Science* 351(6277):aab4113.

[43] Rubin R, Gütig R, Sompolinsky H (2013) Neural coding and decoding with spike times in *Spike Timing: Mechanisms and Function.* (CRC Press), pp. 35–64.

[44] Gütig R (2014) To spike, or when to spike? *Current Opinion in Neurobiology* 25:134–139.

[45] Amit DJ, Gutfreund H, Sompolinsky H (1985) Storing Infinite Numbers of Patterns in a Spin-Glass Model of Neural Networks. *Phys. Rev. Lett.* 55(14):1530–1533.

[46] Tsodyks MV, Feigel'man MV (1988) The Enhanced Storage Capacity in Neural Networks with Low Activity Level. *EPL (Europhysics Letters)* 6(2):101.

[47] Roudi Y, Latham PE (2007) A Balanced Memory Network. *PLOS Computational Biology* 3(9):e141.

[48] Krauth W, Nadal JP, Mezard M (1988) Basins of Attraction in a Perceptron-like Neural Network. *Complex Systems* 2:387–408.

[49] Krauth W, Nadal JP, Mezard M (1988) The roles of stability and symmetry in the dynamics of neural networks. *Journal of Physics A: Mathematical and General* 21(13):2995.

[50] Amit DJ, Treves A (1989) Associative memory neural network with low temporal spiking rates. *Proceedings of the National Academy of Sciences* 86(20):7871–7875.

[51] Golomb D, Rubin N, Sompolinsky H (1990) Willshaw model: Associative memory with sparse coding and low firing rates. *Physical Review A* 41(4):1843–1854.

[52] Hasselmo ME (1993) Acetylcholine and Learning in a Cortical Associative Memory. *Neural Computation* 5(1):32–44.

[53] Barkai E, Bergman RE, Horwitz G, Hasselmo ME (1994) Modulation of associative memory function in a biophysical simulation of rat piriform cortex. *Journal of Neurophysiology* 72(2):659–677.

[54] Kadmon J, Sompolinsky H (2015) Transition to Chaos in Random Neuronal Networks. *Physical Review X* 5(4):041030.

[55] Harish O, Hansel D (2015) Asynchronous Rate Chaos in Spiking Neuronal Circuits. *PLOS Computational Biology* 11(7):e1004266.

[56] Nugent FS, Kauer JA (2008) LTP of GABAergic synapses in the ventral tegmental area and beyond. *The Journal of Physiology* 586(6):1487–1493.

[57] Chevaleyre V, Castillo PE (2003) Heterosynaptic LTD of Hippocampal GABAergic Synapses: A Novel Role of Endocannabinoids in Regulating Excitability. *Neuron* 38(3):461–472.

[58] D'amour JA, Froemke RC (2015) Inhibitory and Excitatory Spike-Timing-Dependent Plasticity in the Auditory Cortex. *Neuron* 86(2):514–528.

[59] McBain CJ, Kauer JA (2009) Presynaptic plasticity: targeted control of inhibitory networks. *Current Opinion in Neurobiology* 19(3):254–262.

[60] Lu Jt, Li Cy, Zhao JP, Poo Mm, Zhang Xh (2007) Spike-Timing-Dependent Plasticity of Neocortical Excitatory Synapses on Inhibitory Interneurons Depends on Target Cell Type. *Journal of Neuroscience* 27(36):9711–9720.

[61] Kullmann DM, Lamsa KP (2007) Long-term synaptic plasticity in hippocampal interneurons. *Nature Reviews Neuroscience* 8(9):687–699.

[62] Lamsa KP, Kullmann DM, Woodin MA (2010) Spike-timing dependent plasticity in inhibitory circuits. *Frontiers in Synaptic Neuroscience* 2.

[63] Larsen RS, Sjöström PJ (2015) Synapse-type-specific plasticity in local circuits. *Current Opinion in Neurobiology* 35:127–135.

[64] Srivastava N, Hinton G, Krizhevsky A, Sutskever I, Salakhutdinov R (2014) Dropout: A Simple Way to Prevent Neural Networks from Overfitting. *J. Mach. Learn. Res.* 15(1):1929–1958.

[65] LeCun Y, Bengio Y, Hinton G (2015) Deep learning. *Nature* 521(7553):436–444.

[66] Marr D (1969) A Theory of Cerebellar Cortex. *Journal of Physiology* 202:437–470.

[67] Albus JS (1971) A theory of cerebellar function. *Mathematical Biosciences* 10(1–2):25–61.

[68] Hennequin G, Everton AJ, Vogels TP (2017) Inhibitory plasticity: Balance, Control and Codependence. *Annual Review of Neuroscience* 40 (in press).

[69] Wilent WB, Nitz DA (2007) Discrete Place Fields of Hippocampal Formation Interneurons. *Journal of Neurophysiology* 97(6):4152–4161.

[70] Andersen M, Dahl J, Liu Z, Vandenberghe L (2011) Interior-point methods for large-scale cone programming. *Optimization for machine learning* pp. 55–83.

[71] Litwin-Kumar A, Harris KD, Axel R, Sompolinsky H, Abbott LF (2017) Optimal Degrees of Synaptic Connectivity. *Neuron* 93(5):1153–1164.e7.

[72] Hunter JD (2007) Matplotlib: A 2d graphics environment. *Computing In Science & Engineering* 9(3):90–95.

[73] Pérez F, Granger BE (2007) IPython: a system for interactive scientific computing. *Computing in Science and Engineering* 9(3):21–29.

[74] Engel A, Broeck C (2001) *Statistical mechanics of learning.* (Cambridge Univ Pr).

Supplementary Information: Balanced Excitation and Inhibition are Required for High-Capacity, Noise-Robust Neuronal Selectivity

Ran Rubin, L.F. Abbott and Haim Sompolinsky

Contents

1 Supplementary Figures

Figure S1: **Numerical measurement of capacity and balanced capacity.** (a) Capacity of sign constrained weights Perceptron, α_c, vs. the fraction of excitatory inputs, f_{exc}, as a fraction of the capacity of an unconstrained Perceptron (see section 3). Theory is depicted in black. Simulations results are shown in blue for $p_{out} = 0.5$ and red for $p_{out} = 0.1$. To measure α_c we measure the probability of the existence of a solution as a function of α. We estimate α_c by the load at which this probability is $1/2$. (b) Capacity of balanced solutions, α_b, as a fraction of α_c vs. $f_{exc} > f^\star_{exc}$. Since κ^{max}_{out} solutions are balanced whenever balanced solutions exist, to measure α_b we measure the probability of finding a balanced κ^{max}_{out} solution i.e. a solution that saturates the upper bound on $|\boldsymbol{w}|$. We estimate α_b by the load at which this probability is $1/2$. In both panels, $N = 3000$, $CV_{exc}/CV_{inh} = \sqrt{2}$.
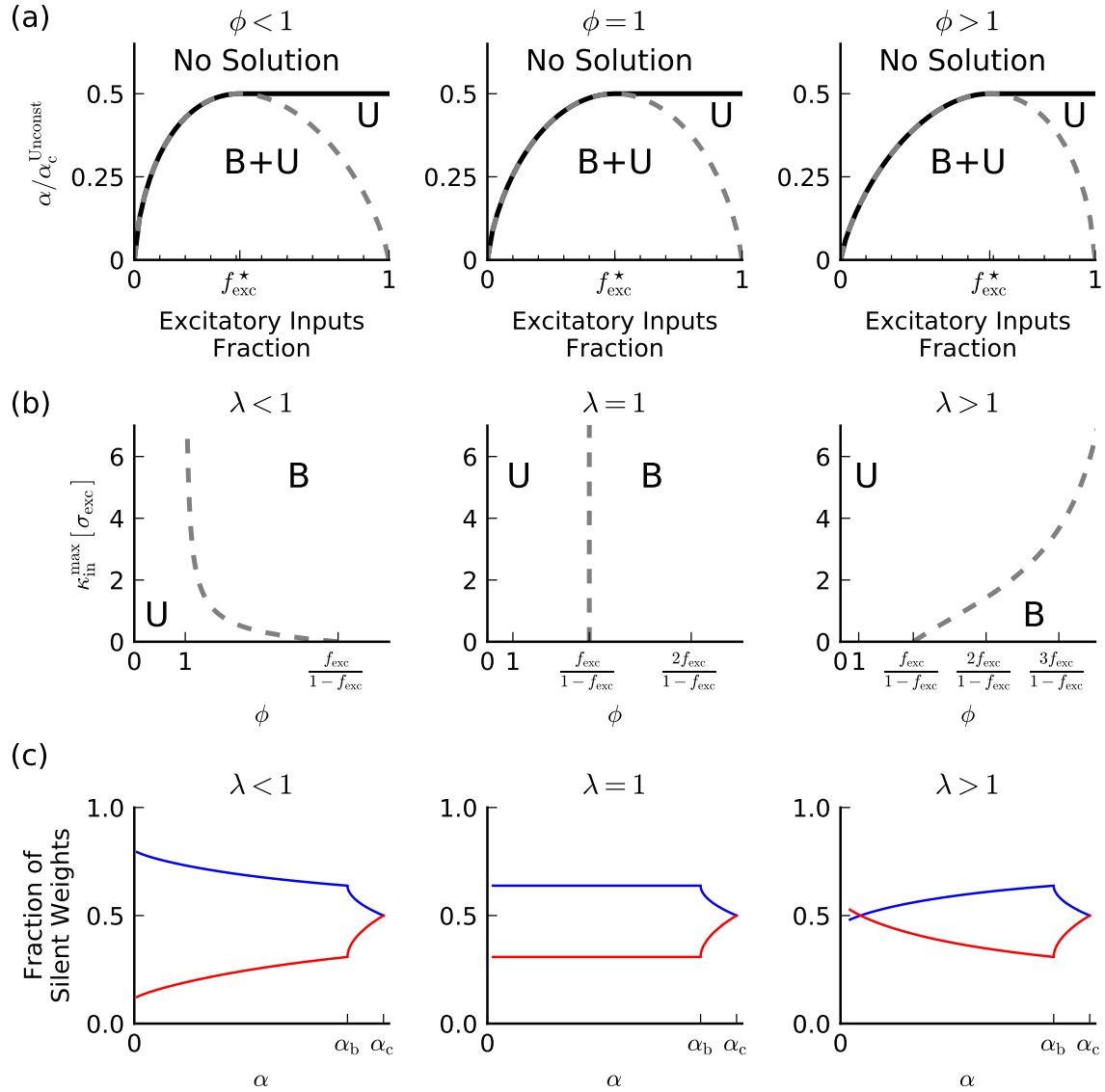
Figure S2: **Effects of input statistics.** (a) Solution type vs. f_{exc} and α (as a fraction of $\alpha_{\text{c}}^{\text{Unconst}}$, see section 3) for different values of $\phi = \text{CV}_{\text{exc}}/\text{CV}_{\text{inh}}$. From left to right $\phi = 1/\sqrt{2}$, 1, $\sqrt{2}$. Lines as in Fig. 2a. (b) Type of **maximal κ_{in} solutions** vs. ϕ and $\kappa_{\text{in}}^{\text{max}}$ for different values of $\lambda = \sigma_{\text{inh}}/\sigma_{\text{exc}}$. For a wide range of ϕ and λ these solutions are unbalanced for all values of $\kappa_{\text{in}}^{\text{max}}$. Here $f_{\text{exc}} = 0.8$ and $\lambda = 1/2$, 1, 2 from left to right. (c) Fraction of silent weights for **maximal κ_{out} solutions** vs. the load for different values of λ. Fraction of silent excitatory weights is shown in blue and fraction of inhibitory silent weights is depicted in red. Here $f_{\text{exc}} = 0.8$, $\phi = \sqrt{2}$, $p_{\text{out}} = 0.1$ and $\lambda = 1/2$, 1, 2 from left to right. Notably, for unbalanced, maximal κ_{in} solutions the fraction of silent weights is constant and equals 0.5 for both excitatory and inhibitory inputs (not shown in figure).
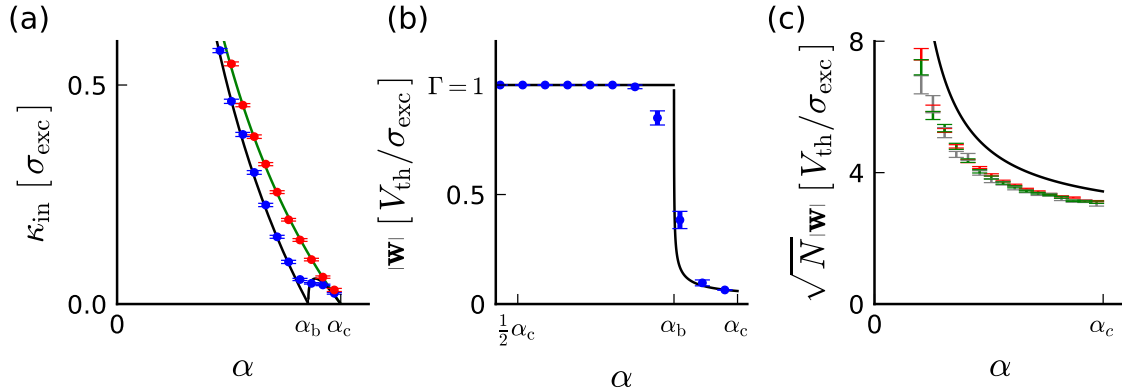
Figure S3: **Properties of maximal output and input robustness solutions.** (a) Input robustness, κ_{in}, vs the load for the maximal κ_{in} solution (red) and the maximal κ_{out} solution (blue). (b) Norm of synaptic weight vector vs. the load for the maximal κ_{out} solution. In the balanced regime ($\alpha < \alpha_{\mathrm{b}}$) the norm saturates its upper bound $\Gamma = 1$. Since the norm is constant, maximizing κ_{out} in the balanced regime is equivalent of maximizing κ_{in} under the constraint $|\boldsymbol{w}| = \Gamma$ (c) Rescaled norm of synaptic weight vector ($\sqrt{N} \, |\boldsymbol{w}|$) vs. the load for the maximal κ_{in} solution. To demonstrate the $1/\sqrt{N}$ scaling of the weight vector norm, colors depict results for $N = 750$ (gray), $N = 1500$ (green) and $N = 3000$ (red). In all panels lines depict theoretical prediction. $f_{\mathrm{exc}} = 0.8$, $p_{\mathrm{out}} = 0.1$, $\phi = \mathrm{CV}_{\mathrm{exc}}/\mathrm{CV}_{\mathrm{inh}} = \sqrt{2}$, $\lambda = \sigma_{\mathrm{inh}}/\sigma_{\mathrm{exc}} = 2$, results are averaged over 100 samples.
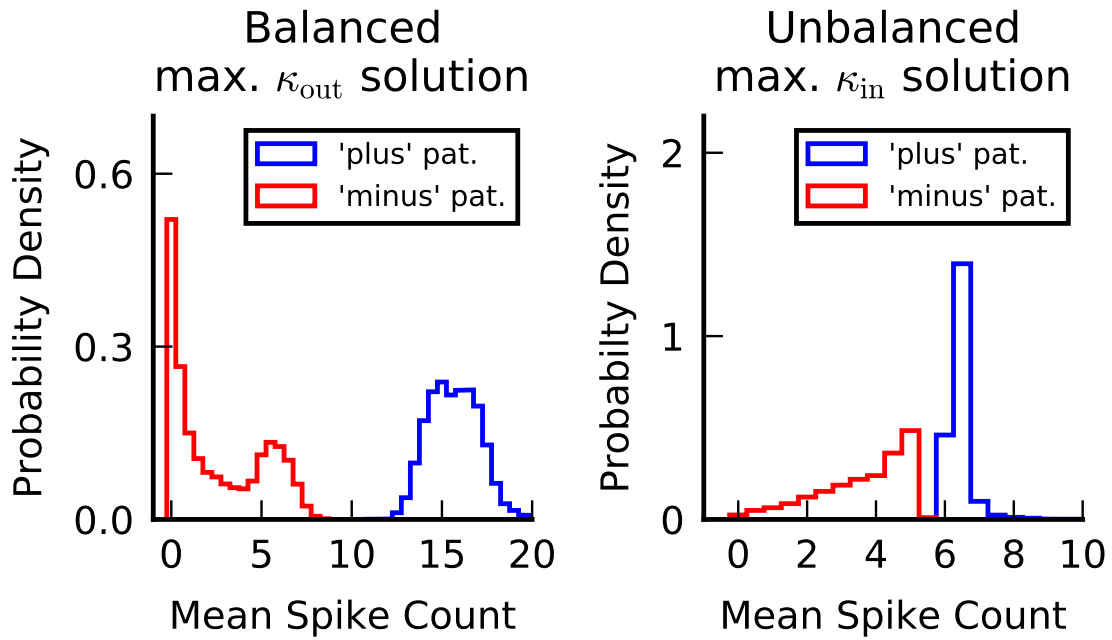
Figure S4: **Neuronal selectivity for a spiking neuron.** Both panels depict the histograms of the mean output spike count for patterns belonging to the 'plus' (blue) and 'minus' (red) classes of an LIF neuron with balanced weights maximizing κ_{out} (left) and unbalanced weights maximizing κ_{in}. Here the magnitude of the output noise is zero. In both cases the mean output spike count can be used to correctly classify the patterns. For parameters used see Fig. 3.
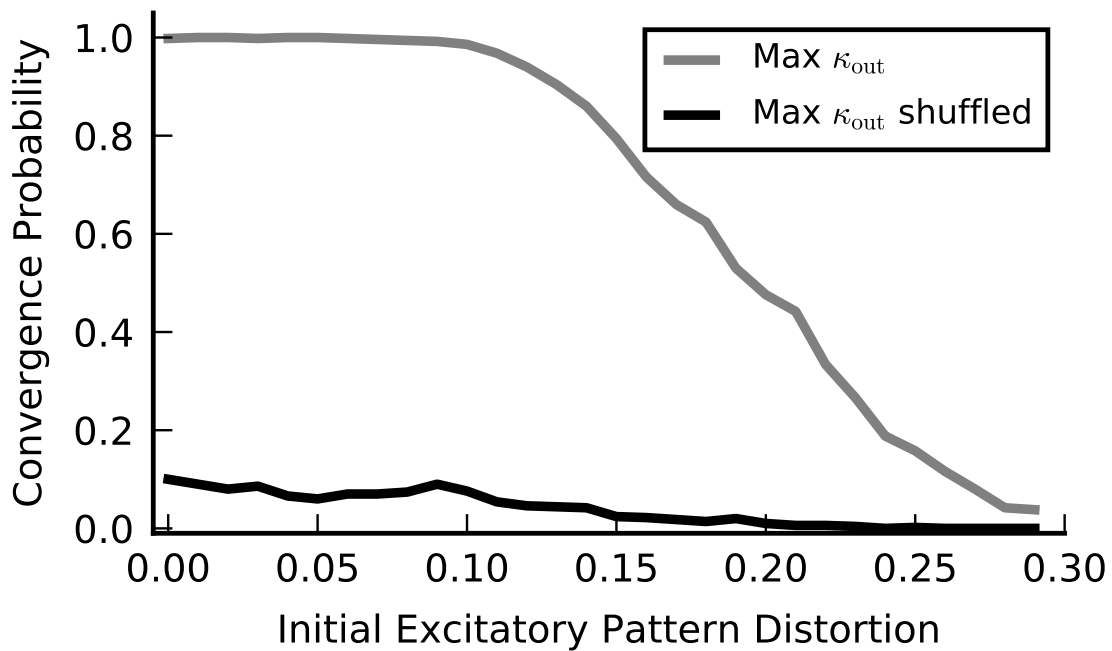
Figure S5: **Effect of shuffling learned inhibitory weights in recurrent networks with non learned inhibitory activity.** Gray line depicts the performance of the a network with random E to I and I to I connection and learned E to E and I to E connections (see section 6, same as gray line in Fig. 5d). Black line depicts the performance of the same network with the inhibitory weights of each excitatory neuron randomly shuffled. Thus the distribution of inhibitory synaptic weights for each excitatory neurons is identical in both cases. This results shows that the learned inhibitory weight are important for network performance and stability.
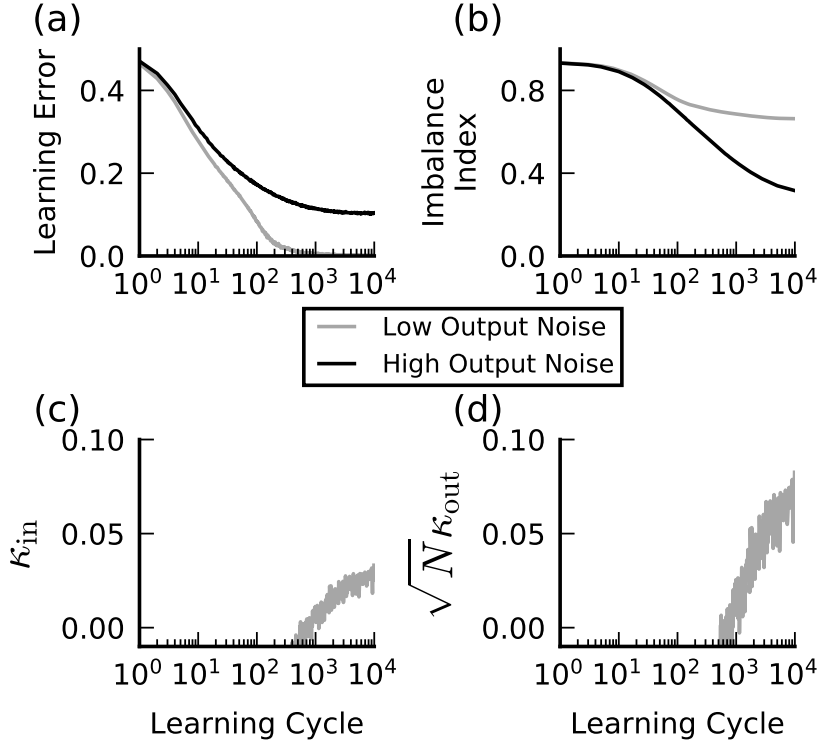
Figure S6: **Perceptron learning with input and output noise for $\alpha_{\mathrm{b}} < \alpha < \alpha_{\mathrm{c}}$.** All panels depict the outcome of simple perceptron learning for a noisy neuron (Methods) under low output noise conditions ($\sigma_{\mathrm{out}} = 0.01/\sqrt{N}$, black) and high output noise conditions ($\sigma_{\mathrm{out}} = 0.01$, gray). Except σ_{out} all model and learning parameters are identical for the two conditions (including $\sigma_{\mathrm{in}} = 0.01$). (a) Mean training error vs. learning cycle. At each cycle all the learned input patterns are presented once. (b) Mean imbalance index vs. learning cycle. IB remains of order 1 under low output noise conditions and drops to lower values under high output noise conditions. (c) Mean input robustness (κ_{in}) vs. learning cycle. (d) Mean rescaled output robustness ($\sqrt{N}\kappa_{\mathrm{out}}$) vs. learning cycle. The error decays and plateaus at its minimal value under both low and high output noise conditions, however for high output noise the error remains substantial. Both output and input robustness are negative under the high output noise conditions (The learning does not find a weights vector that performs the classification of the noise free patterns correctly). Input and output robustness are positive when the output noise scales at most as $1/\sqrt{N}$. Random patterns are binary pattern $x_i^{\mu} \in \{0,1\}$ with equal probabilities and an even split of 'plus' and 'minus' patterns. $N = 3000$, $P = 2400$. Learning algorithm parameters: $\varepsilon = 10^{-8}$, $\rho = 0.02/N$, $\sigma_{\mathrm{in}} = 0.01$. Results are averaged over 50 samples.

2   Finding maximal κ_{in} and maximal κ_{out} solutions

Here we describe how finding the maximal κ_{in} and maximal κ_{out} solutions can be expressed as convex conic optimization problems. This allows us to efficiently validate the theoretical results. As noted in the main text, maximizing κ_{in} is equivalent to maximizing the margin of the solution's weight vector as is done by Support Vector Machines [38]. However, to our knowledge, the application of conic optimization tools for maximizing κ_{out} is a novel contribution of our work.

Solution weight vectors, $\boldsymbol{w}$, with input robustness κ_{in}, or output robustness κ_{out}, satisfy the following inequalities:

$$\forall \mu \ y^{\mu} \left(\boldsymbol{w}^T \boldsymbol{x}^{\mu} - V_{\text{th}} \right) \geq D \tag{S.1}$$

where $D_{\text{in}} = |\boldsymbol{w}| \, \kappa_{\text{in}}$ and $D_{\text{out}} = \kappa_{\text{out}}$ (here we assume without loss of generality that $V_{\text{rest}} = 0$).

For each solution $\boldsymbol{w}$ we define effective weights, $\boldsymbol{u}$, and effective threshold b (the so called canonical weights and threshold [38]) given by

$$u_i = \Lambda w_i \tag{S.2}$$

$$b = \Lambda V_{\text{th}} \tag{S.3}$$

where $\Lambda > 0$ is chosen such that $\Lambda D = 1$ (for either D_{in} or D_{out}).

Together with the sign and norm constraints on the weights, $\boldsymbol{u}$ and b must satisfy the linear constraints

$$\forall \mu \ y^{\mu} \left(\boldsymbol{u}^T \boldsymbol{x}^{\mu} - b \right) \geq 1 \tag{S.4}$$
$$\forall i \ s_i u_i \geq 0$$
$$b \geq 0$$

where $s_i = 1$ if w_i is excitatory and $s_i = -1$ if w_i is inhibitory, and the quadratic constraint

$$|\boldsymbol{u}|^2 \leq b^2 \Gamma^2 / V_{\text{th}}^2, \tag{S.5}$$

which enforces the constraint $|\boldsymbol{w}| \leq \Gamma$.

For the effective weights and threshold, κ_{in} is given by $\kappa_{\text{in}} = \frac{1}{|\boldsymbol{u}|}$ and κ_{out} is given by $\kappa_{\text{out}} = \frac{V_{\text{th}}}{b}$. Thus, maximizing κ_{in} is equivalent to minimizing $|\boldsymbol{u}|$ and maximizing κ_{out} is equivalent to minimizing b. We therefor define a minimization cost function $E(\boldsymbol{u}, b)$ that is given by

$$E_{\text{in}}(\boldsymbol{u}, b) = \frac{1}{2} \boldsymbol{u}^T \boldsymbol{u} \ , \tag{S.6}$$

for the $\kappa_{\text{in}}^{\text{max}}$ solution, and

$$E_{\text{out}}(\boldsymbol{u}, b) = b \ , \tag{S.7}$$

for the $\kappa_{\text{out}}^{\text{max}}$ solution.

To find the maximal κ_{in} or maximal κ_{out} solution we solve the conic program:

$$\min_{u,b,\tau} E(\boldsymbol{u}, b) + \beta \tau \tag{S.8}$$

in the limit of $\beta \to \infty$, subject to

$$\forall \mu \ y^{\mu} \left(\boldsymbol{u}^T \boldsymbol{x}^{\mu} - b \right) \geq 1 - \tau \tag{S.9}$$
$$\forall i \ s_i u_i \geq 0$$
$$b \geq 0$$
$$\tau \geq 0$$
$$b^2 \Gamma^2 / V_{\text{th}}^2 \geq |\boldsymbol{u}|^2 \ .$$

τ is a global regularization variable that insures the existence of a solution to the optimization problem (eqs. S.8 and S.9) even when the linear constraints (S.4) are not realizable. In practice it is sufficient to set β to be a large constant (we set $\beta = 10^5$). If the optimal value of τ is zero the solution corresponds to the optimal perceptron solution for the classification task. If the optimal value of τ is greater then zero, it indicates that the labeled patterns are not linearly separable and that there is no zero error solution to the classification task. Given that a solution with $\tau = 0$ is found, the optimal weights are given by $\boldsymbol{w} = V_{\text{th}} \boldsymbol{u}/b$.

3 Capacity for non-even split of 'plus' and 'minus' patterns

The capacity of a perceptron with no sign constraints on synaptic weights for classification of random patterns is a function of the fraction of 'plus' patterns in the desired classification, p_{out} [19, 21, 20] and is given by

$$\alpha_{\text{c}}^{\text{Unconst.}} = \left[p_{\text{out}} \int_{-\infty}^{\Delta} Dt \left(t - \Delta \right)^2 + (1 - p_{\text{out}}) \int_{\Delta}^{\infty} Dt \left(t - \Delta \right)^2 \right]^{-1}$$

where Dt is the Gaussian integration measure, $Dt = \frac{e^{-\frac{t^2}{2}}}{\sqrt{2\pi}} dt$ and the order parameter Δ is given by the solution to the equation

$$0 = p_{\text{out}} \int_{-\infty}^{\Delta} Dt \left(t - \Delta \right) + (1 - p_{\text{out}}) \int_{\Delta}^{\infty} Dt \left(t - \Delta \right) \ .$$

Fig. S1(a) depicts the theoretical and measured α_{c} of our 'constrained' perceptron as a fraction of the corresponding unconstrained capacity vs. f_{exc} for two values of p_{out}. Fig. S1(b) depicts theoretical and measured of α_{b} as a fraction of α_{c} for two values of p_{out}.

4 Effects of excitatory and inhibitory input statistics

Our results depend, of course, on parameters, but in a fairly reduced way. In particular, the properties we discuss depend on the ratio of the inputs standard deviations, $\lambda = \sigma_{\text{inh}}/\sigma_{\text{exc}}$ and the ratio of their coefficients of variation, $\phi = \text{CV}_{\text{exc}}/\text{CV}_{\text{inh}}$ (see section 7). As discussed in the main text ϕ determines the value of the optimal fraction of excitatory synapses, $f_{\text{exc}}^{\star}$ which can be written as $f_{\text{exc}}^{\star} = \phi/ \left(1 + \phi \right)$ (see eq. 2 in the main text). Thus the shape of the phase diagram changes with ϕ (Fig. S2a). The parameter λ has more subtle effects. We note here the main effect λ has on the maximal κ_{in} and maximal κ_{out} solutions.

4.1 Balanced and unbalanced maximal κ_{in} solutions

The **maximal κ_{in} solutions** can be either balanced or unbalanced depending on f_{exc}, ϕ, λ and the value of $\kappa_{\mathrm{in}}^{\mathrm{max}}$ (see example in Fig. S2b). Importantly, for a wide range of reasonable parameters (For example, $\phi \leq f_{\mathrm{exc}}/(1 - f_{\mathrm{exc}})$ and $\lambda \geq 1$) the $\kappa_{\mathrm{in}}^{\mathrm{max}}$ solution is unbalanced for all values of $\kappa_{\mathrm{in}}^{\mathrm{max}}$.

4.2 Fraction of 'silent' weights in maximal κ_{in} and maximal κ_{out} solutions

As noted in previous studies [24, 26], a prominent feature of 'critical' solutions with sign constraint weights, such as the maximal κ_{in} and maximal κ_{out} solutions, is that a finite fraction of the synapses are 'silent' i.e. $w_i = 0$. Our theory allows us to derive the full distribution of synaptic efficacies (section 7.3.9) and calculate the fraction of silent weights for each solution. For the maximal κ_{out} solutions in the unbalanced regime ($\alpha_{\mathrm{b}} < \alpha < \alpha_{\mathrm{c}}$), the fraction of excitatory (inhibitory) silent weights is always larger (smaller) then $1/2$ (Fig. S2c). However, in the balanced regime ($\alpha < \alpha_{\mathrm{b}}$) the qualitative behavior depends on λ (see Fig. S2c). Interestingly, for **unbalanced maximal κ_{in} solutions** the fraction of silent weights is constant and equals $1/2$ for both excitatory and inhibitory inputs (see sections 7.3.7 and 7.3.9).

4.3 Tuning properties of cortical neurons suggest that in cortex $f_{\mathrm{exc}}^\star > 0.5$

In cortical circuits, inhibitory neurons tend to fire with higher firing rates and are thought to be more broadly tuned than excitatory neurons implying, under reasonable assumptions, that both λ and ϕ are greater than 1 leading to $f_{\mathrm{exc}}^\star > 0.5$.

To see this, we consider input neurons with Gaussian tuning curves to some external stimulus variable $\varphi \in [0, 1]$, i.e. the mean response, x_i, of neuron i to stimulus φ is given by

$$x_i = A_i \exp\left[-\left(\varphi - \varphi_i^{\mathrm{pref}}\right)^2 / \left(2\delta_i^2\right)\right] , \tag{S.10}$$

where A_i, $\varphi_i^{\mathrm{pref}}$ and δ_i characterize the response properties of the neuron. Assuming that φ is distributed uniformly, and, for simplicity, that $\delta_i \ll 1$, the mean and variance of the neurons' responses are given by:

$$\bar{x}_i = \sqrt{2\pi} A_i \delta_i , \tag{S.11}$$

and

$$\sigma_i^2 \simeq A^2 \delta \sqrt{\pi} , \tag{S.12}$$

where we neglect terms of order δ^2. We now assume that $A_i = A_{\mathrm{exc}}$ and $\delta_i = \delta_{\mathrm{exc}}$ if neuron i is excitatory and that $A_i = A_{\mathrm{inh}}$ and $\delta_i = \delta_{\mathrm{inh}}$ if neuron i is inhibitory. Further, we assume that inhibitory neurons respond with a higher firing rate ($A_{\mathrm{inh}} > A_{\mathrm{exc}}$) and are more broadly tuned ($\delta_{\mathrm{inh}} > \delta_{\mathrm{exc}}$). In this case we have

$$\lambda = \frac{A_{\mathrm{inh}}\sqrt{\delta_{\mathrm{inh}}}}{A_{\mathrm{exc}}\sqrt{\delta_{\mathrm{exc}}}} > 1 , \tag{S.13}$$

and

$$\phi = \sqrt{\frac{\delta_{\mathrm{inh}}}{\delta_{\mathrm{exc}}}} > 1 . \tag{S.14}$$

5 $\kappa_{\text{out}}^{\text{max}}$ and $\kappa_{\text{in}}^{\text{max}}$ solutions in purely excitatory networks

In purely excitatory networks ($f_{\text{exc}} = 1$) all solutions are unbalanced and output robustness can be achieved by sparse input [24] or tonic inhibition [27]. However, the distinction between output robustness and input robustness still apply and, surprisingly, maximizing either κ_{in} or κ_{out} leads to two different solutions with qualitatively different properties.

In particular, as noted in [24, 26], the fraction of silent weights of the $\kappa_{\text{out}}^{\text{max}}$ solutions increases as the load decreases. Thus, if the network implements the maximal κ_{out} solution, network connectivity, as measured in pairwise stimulation experiment, is expected to be sparse. However, for the maximal κ_{in} solution the fraction of silent weights is constant and remains $1/2$ for all values of the load. Thus, measured network connectivity is expected to be higher.

Establishing correspondence between theory and experiment in this case is confounded by the difficulty to experimentally distinguish between silent synapses and completely absent synapses that were never available as inputs for the post synaptic neuron during learning.

6 Recurrent networks with non-learned inhibition

In our basic model for an associative memory network we assume that the activity of both excitatory and inhibitory neuron is specified in the desired memory states and that all network connections are learned. Both of these assumptions can be modified creating new scenarios with different computational properties.

First we assume that memory state is only specified by the activity of excitatory neurons and that the memory is recalled when the activity of excitatory neurons matches the memory state regardless of the activity of inhibitory neurons. The problem of learning in such a network is computationally hard since the learning needs to optimize the activity of the inhibitory neurons using the full connectivity matrix. In our work we do not address this scenario. Instead we forgo the assumption that excitatory and inhibitory connections onto inhibitory neurons are learned and replace them with randomly chosen connections, i.e. assume that E to I and I to I connections are not learned and random.

6.1 Choosing random synapses for inhibitory neurons

In this scenario the activity of inhibitory neurons is determined by the network dynamics. We consider random I to I and E to I weights with means J_{II} and J_{IE} and standard deviations $\sigma_{J_{\text{II}}}$ and $\sigma_{J_{\text{IE}}}$. We will examine the distribution of inhibitory neurons' membrane potential given that the activity of excitatory neurons is held at a memory state in which $p_{\text{out}}^{\text{exc}} N$ neurons are active. When N is large, this distribution is Gaussian and we assume correlations are weak. Thus, the mean activity in the network is the probability that the membrane potential is above threshold and is given by the equation

$$m_{\text{I}} = H\left(\frac{V_{\text{th}} - \langle V \rangle}{\sqrt{\sigma^2\left(V\right)}}\right) \,, \tag{S.15}$$

where $H(x) = \int_x^\infty \frac{e^{-\frac{y^2}{2}}}{\sqrt{2\pi}} \mathrm{d}y$, and $\langle V \rangle$ and $\sigma^2(V)$ are the mean and variance of the membrane potential of inhibitory neurons, respectively.

On the other hand, given the mean activity, m_I, the mean and variance of the membrane potentials are given by

$$\langle V \rangle = N\left(p_\mathrm{out}^\mathrm{exc} g_\mathrm{exc} J_\mathrm{IE} - m_\mathrm{I}\left(1 - g_\mathrm{exc}\right) J_\mathrm{II}\right) \tag{S.16}$$

$$\sigma^2(V) = N\left(\left[\sigma_{J_\mathrm{IE}}^2 + \left(1 - p_\mathrm{out}^\mathrm{exc}\right) J_\mathrm{IE}^2\right] p_\mathrm{out}^\mathrm{exc} g_\mathrm{exc} + \left[\sigma_{J_\mathrm{II}}^2 + \left(1 - m_\mathrm{I}\right) J_\mathrm{II}^2\right] m_\mathrm{I}\left(1 - g_\mathrm{exc}\right)\right) . \tag{S.17}$$

Together, eqs. (S.15)-(S.17) define the relations between m_I, J_II, J_IE, σ_{J_IE} and σ_{J_II}.

In our simulations we set m_I and the mean and variance of the I to I connections, and choose the mean and variance of the E to I connections according to the solution of (S.15) (When N is large J_IE is given by $N J_\mathrm{IE} \simeq \left(V_\mathrm{th} + m_\mathrm{I} N\left(1 - g_\mathrm{exc}\right) J_\mathrm{II}\right) / \left(g_\mathrm{exc} p_\mathrm{out}^\mathrm{exc}\right)$). In particular, we choose an inhibitory network with binary weights in which each inhibitory neuron projects to another inhibitory neuron with probability p_II with synaptic efficacy $j_\mathrm{II} = 1/\left(\sqrt{N} p_\mathrm{II}\right)$. Each excitatory neuron project to an inhibitory neuron with probability p_IE with synaptic efficacy j_IE that ensures that the mean inhibitory activity level at the memory states is m_I.

In this parameter regime, the inhibitory subnetwork exhibits asynchronous activity, with mean activity m_I, at the excitatory memory states. However, different memory states lead to different asynchronous states.

6.2   Training set definition

Excitatory neurons need to learn to remain stationary at the desired memory states given the network activity at this state. However, since the activity of the inhibitory subnetwork is not stationary at the desired memory states, the training set for learning is not well defined.

To properly define the training set, we sample n_sample instances of the generated inhibitory activity for each memory state when the activity of the excitatory neuron is clipped to this memory state. Sampling was performed by running the inhibitory network dynamics and recording the state of the inhibitory neurons after $T = 100N$ time steps. We then use the sampled activity patterns together with the excitatory memory states as an extended training set (with Pn_sample patterns) for the excitatory neurons.

6.3   Learned network stability

The non fixed point dynamics of the inhibitory subnetwork implies that the convergence of the learning on the training set does not entail that the memory states themselves are dynamically stable, in contrast to our prior model in which inhibitory neurons learn their synaptic weights. Therefor, after training we measure the probabilities that patterns are stable. This is done by the following procedure: First we run the network dynamics (with $\sigma_\mathrm{out} = 0$) when the excitatory neurons' activity is clipped to the memory state, for $T_\mathrm{init} = 50N$ time steps. We then release the excitatory neurons to evolve according to the natural network dynamics and observe if their activity remain in the vicinity of the memory state for $T = 500N$ time steps. In a similar way we test the basins of attractions, starting the excitatory network from a distorted version of the memory state instead of the memory state itself.

6.4 Learning only E to E connections

First we consider the case in which I to E connections are random: Each inhibitory neuron project to an excitatory neuron with probability p_{EI} with synaptic efficacy $j_{\mathrm{EI}} = 1/\left(\sqrt{N}p_{\mathrm{EI}}\right)$. We then try to find appropriate E to E connection using the learning scheme described above. We find that the pattern to pattern fluctuations in the inhibitory feedback due to the variance of the I to E connections, and the variance in the inhibitory network neurons' activation is substantial and of the same order of the signal differentiating the memory states. In fact, in this scenario the parameters we consider ($N = 2000$, $P = 1000$, $g_{\mathrm{exc}} = 0.8$, $p_{\mathrm{out}}^{\mathrm{exc}} = 0.15$, $p_{\mathrm{II}} = 1/2$, $p_{\mathrm{IE}} = 1/2$, $m_{\mathrm{I}} = 0.4$, $p_{\mathrm{EI}} = 1/2$, $n_{\mathrm{sample}} = 40$) are above the system's memory capacity and we are unable to find appropriate excitatory weights which implement the desired memory states for the training set. We conclude that this form of balancing inhibitory feedback is too restrictive due to the heterogeneity of I to E connections and variability of inhibitory neurons' activity.

6.5 Learning both E to E and I to E connections

In this scenario we find the maximal κ_{out} solution for the extended training set described above. For the parameters used ($N = 2000$, $P = 1000$, $g_{\mathrm{exc}} = 0.8$, $p_{\mathrm{out}}^{\mathrm{exc}} = 0.15$, $p_{\mathrm{II}} = 1/2$, $p_{\mathrm{IE}} = 1/2$, $m_{\mathrm{I}} = 0.4$, $n_{\mathrm{sample}} = 40$) we are able to find solutions that implement all the desired memory states for the extended training set. In addition, we find that the excitatory memory states are dynamically stable with very high probability (we did not observe any unstable pattern). For numerical results see Fig. 5 and Fig S5.

7 Replica theory for sign and norm constrained perceptron

We use the Replica method [74] to calculate the system's typical properties. For the Perceptron architecture the replica symmetric solution has been shown to be stable and exact [19, 21, 20].

Given a set of P patterns, $\boldsymbol{x}^{\mu}$, and desired labels $y^{\mu} = \pm 1$ for $\mu = 1, 2, \ldots, P$, the Gardner volume for is given by:

$$V_{\mathrm{G}} = \int \mathcal{D}\left(\boldsymbol{w}\right) \prod_{\mu=1}^{P} \Theta\left[y^{\mu}\left(w^{\mathrm{T}}\boldsymbol{x}^{\mu} - V_{\mathrm{th}}\right) - K\right] \ , \tag{S.18}$$

where $\Theta\left[x\right]$ is the Heaviside step function and $\mathcal{D}\left(\boldsymbol{w}\right)$ is an integration domain obeying the sign and norm constraint $|\boldsymbol{w}| \leq \Gamma$.

We assume input pattern and labels are drawn independently from distribution with non negative means $\bar{x}_{\mathrm{exc(inh)}}$ and standard deviation $\sigma_{\mathrm{exc(inh)}}$. Labels are independently drawn from a binary distribution with $\Pr\left(y^{\mu} = 1\right) = p_{\mathrm{out}}$ and $\Pr\left(y^{\mu} = -1\right) = 1 - p_{\mathrm{out}}$.

We handle both input and output robustness criteria by using different K for each case:

$$K_{\mathrm{in}} = |\boldsymbol{w}|\sigma_{\mathrm{exc}}\kappa_{\mathrm{in}} \tag{S.19}$$
$$K_{\mathrm{out}} = V_{\mathrm{th}}\kappa_{\mathrm{out}} \ ,$$

where, here, κ_{in} and κ_{out} are dimensionless numbers representing the input robustness in units of σ_{exc} and the output robustness in units of V_{th} respectively.

Further, we define the parameters:

$$\lambda = \frac{\sigma_{\text{inh}}}{\sigma_{\text{exc}}}, \;\; \eta = \frac{\bar{x}_{\text{inh}}}{\bar{x}_{\text{exc}}} \; , \tag{S.20}$$

and

$$\phi = \frac{\text{CV}_{\text{exc}}}{\text{CV}_{\text{inh}}} \; . \tag{S.21}$$

7.1 The order parameters

We calculate the mean logarithm of the Gardner volume $\langle\langle \ln V_{\text{G}} \rangle_x \rangle_y$ averaged over the excitatory and inhibitory input distributions, and the desired label distribution. The result of the calculation is expressing $\langle\langle \ln V_{\text{G}} \rangle_x \rangle_y$ as a stationary phase integral over a free energy that is a function of several order parameters. The value of the order parameters is determined by the saddle point equations of the free energy.

In our model the saddle point equations are a system of six equations for the six order parameter: q, Q, θ, Δ, B and C.

The order parameters q, Q, θ, and Δ have a straight forward physical interpretation.

The parameter q is the mean typical correlation coefficient between the V_{PSP}'s elicited by two different solutions to the same classification task: given two typical solution weight vectors $\boldsymbol{w}^\alpha$ and $\boldsymbol{w}^\beta$, q is given by

$$q = \frac{\sum_{i=1}^{N} \lambda_i^2 w_i^\alpha w_i^\beta}{\sqrt{\left(\sum_{i=1}^{N} \lambda_i^2 w_i^{\alpha 2}\right)\left(\sum_{i=1}^{N} \lambda_i^2 w_i^{\beta 2}\right)}} \; , \tag{S.22}$$

where $\lambda_i = 1$ if w_i is excitatory and $\lambda_i = \lambda$ if w_i is inhibitory.

Given a typical solution $\boldsymbol{w}$, the physical interpretation of Q and θ is given by

$$Q = \frac{\sum_{i=1}^{N} \lambda_i^2 w_i^2}{\sum_{i=1}^{N} w_i^2} \tag{S.23}$$

$$\theta = \frac{V_{\text{th}}}{\sigma_{\text{exc}}} \left(\sum_{i=1}^{N} \lambda_i^2 w_i^2\right)^{-\frac{1}{2}} . \tag{S.24}$$

The norm constraint on the weights is satisfied as long as

$$\theta \geq \frac{V_{\text{th}}}{\sigma_{\text{exc}} \Gamma \sqrt{Q}} \; . \tag{S.25}$$

Thus, there are two types of solutions. One in which the value of θ is determined by the saddle point equation (unbalanced solutions) and the other in which θ is clipped to its lower bound

43

value (balanced solutions). Notice that q and Q remain of order 1 for any scaling of $|\boldsymbol{w}|$ while θ scales as $\sqrt{N}$ when $|\boldsymbol{w}|$ is of order $1/\sqrt{N}$ and is of order 1 when $|\boldsymbol{w}|$ is of order 1.

The physical interpretation of Δ can be expressed through the following relation

$$\Delta = \theta \left(1 - \frac{\bar{x}_{\text{exc}} \sum_{i=1}^{N} \eta_i w_i}{V_{\text{th}}} \right) , \tag{S.26}$$

where $\eta_i = 1$ if w_i is excitatory and $\eta_i = \eta$ if w_i is inhibitory.

7.2   Summary of main results

Before describing the full saddle point (SP) equations and their various solutions in detail we will provide a brief general summary of the results that would hopefully provide some flavor of the derivations for the interested reader.

Since θ is bounded from bellow by $V_{\text{th}}/\left(\sigma_{\text{exc}}\Gamma\sqrt{Q}\right)$ we have two sets of SP equations which we term the balanced and the unbalanced sets. In both sets, given the free energy $\mathcal{F}\left(Q, q, \Delta, \theta, B, C\right)$, five of the SP equations are given by

$$\frac{\partial \mathcal{F}}{\partial Q} = \frac{\partial \mathcal{F}}{\partial q} = \frac{\partial \mathcal{F}}{\partial \Delta} = \frac{\partial \mathcal{F}}{\partial B} = \frac{\partial \mathcal{F}}{\partial C} = 0 . \tag{S.27}$$

The sixth equations is

$$\frac{\partial \mathcal{F}}{\partial \theta} = 0 \tag{S.28}$$

in the unbalanced set and is

$$\theta = \frac{V_{\text{th}}}{\sigma_{\text{exc}}\Gamma\sqrt{Q}} \tag{S.29}$$

in the balanced set. Importantly, we find that eq. S.28 has solutions only when $\theta \sim \sqrt{N}$ which implies $|\boldsymbol{w}| \sim 1/\sqrt{N}$, and eq. S.29 implies $|\boldsymbol{w}| = \Gamma \sim \mathcal{O}\left(1\right)$, justifying the naming of the two sets. The solutions to the two sets of SP equations define the range of possible values of α, κ_{in} and κ_{out} that permits the existence of solution weight vectors. There are a number of interesting cases that we analyze below.

We first consider the solutions of the SP equations for zero κ_{out} and κ_{in}. In this case the SP describes the typical solutions that dominate the Gardner volume. Since the N-dim. volume of balanced solutions with $|\boldsymbol{w}| \sim 1$ is exponentially larger than the volume of unbalanced solutions with $|\boldsymbol{w}| \sim 1/\sqrt{N}$ we expect that balanced solutions will dominate the Gardner volume whenever they exist. Indeed, solving the two sets of SP equations we find that solutions to the balanced set exist only for $\alpha < \alpha_{\text{b}}$ while solutions for the unbalanced set exist only for $\alpha_{\text{b}} < \alpha < \alpha_{\text{c}}$.

Next, we examine the values of κ_{out} that permits solutions to the balanced and unbalanced sets of SP equations. Importantly, we show that the unbalanced set can only be solved for $\kappa_{\text{out}} \propto 1/\sqrt{N}$. Thus, unbalanced solutions can not have κ_{out} of $\mathcal{O}\left(1\right)$ or conversely all solutions with κ_{out} of $\mathcal{O}\left(1\right)$ are balanced.

Of particular interest are the so called 'critical' solutions for which $q \to 1$. At this limit the typical correlation coefficient between the V_{PSP}'s elicited by two different solutions to the

same classification task approaches unity, which implies that only one solution exist and the Gardner volume shrinks to zero. Thus, for a given κ_{in} or κ_{out}, the value of α for which $q \to 1$ is the maximal load for which solutions exist. In this case, the SP describes the properties of the maximal κ_{out} or κ_{in} solutions.

The structure of the equations in this limit is relatively simple. First, the order parameter Δ is given by the solutions to

$$0 = p_{\text{out}} \int_{-\infty}^{\Delta + \tilde{K}} Dt \left(t - \Delta - \tilde{K} \right) + (1 - p_{\text{out}}) \int_{\Delta - \tilde{K}}^{\infty} Dt \left(t - \Delta + \tilde{K} \right) \tag{S.30}$$

with the robustness parameter $\tilde{K}$ being $\tilde{K}_{\text{in}} = \kappa_{\text{in}}/\sqrt{Q}$ or $\tilde{K}_{\text{out}} = \theta \kappa_{\text{out}}$ and the integration measure, Dt, is given by $Dt = \frac{e^{-\frac{t^2}{2}}}{\sqrt{2\pi}} dt$. Second, we find a simple relation between critical loads of the constrained perceptron considered here and the critical loads of the classic unconstrained perceptron, $\alpha^{\text{Unconst.}}$:

$$\alpha = 2C\alpha^{\text{Unconst.}} . \tag{S.31}$$

$\alpha^{\text{Unconst.}}$ is given by

$$\alpha^{\text{Unconst.}} = \left[p_{\text{out}} \int_{-\infty}^{\Delta + \tilde{K}} Dt \left(t - \Delta - \tilde{K} \right)^2 + (1 - p_{\text{out}}) \int_{\Delta - \tilde{K}}^{\infty} Dt \left(t - \Delta + \tilde{K} \right)^2 \right]^{-1}, \tag{S.32}$$

which is indeed the critical load of an unconstrained perceptron with a given margin $\tilde{K}$ (see [20]). Finding the critical load is then reduced to solving for the order parameter C. For each value of $\kappa_{\text{in}} > 0$ or $\kappa_{\text{out}} > 0$ only one set of SP equations can be solved, determining if the maximal κ_{in} or κ_{out} solutions are balanced or unbalanced. By examining the range of solutions for each set we can find the value of $\kappa_{\text{in}}^{\text{max}}$ and $\kappa_{\text{out}}^{\text{max}}$ for any α and determine that (a) the maximal κ_{out} solution is balanced for $\alpha \leq \alpha_{\text{b}}$ and unbalanced for $\alpha_{\text{b}} < \alpha < \alpha_{\text{c}}$ and (b) that for a wide range of parameters the maximal κ_{in} is unbalanced for all $\alpha < \alpha_{\text{c}}$. In addition, we find that for $\alpha_{\text{b}} < \alpha < \alpha_{\text{c}}$, $\kappa_{\text{out}}^{\text{max}}$ is given by

$$\kappa_{\text{out}}^{\text{max}} = \frac{\sigma_{\text{exc}}}{\bar{x}_{\text{exc}} \sqrt{N}} \kappa_0 \tag{S.33}$$

where κ_0 is finite and larger than zero when α approaches α_{b} from above and κ_0 approaches zero when α approaches α_{c}. The above result implies that output robustness can be increased when the tuning of the input is increased. As we discuss in the main text in the context of neuronal selectivity in purely excitatory circuits, sparse input activity is one way to increase the input tuning. If we consider sparse binary inputs with mean activity level $s \ll 1$ the output robustness will be given by $\kappa_0 \sqrt{(1 - s)/sN} \simeq \kappa_0/\sqrt{sN}$.

Finally, we consider the solutions of the SP equations in the critical limit ($q \to 1$) for $\kappa_{\text{in}} = \kappa_{\text{out}} = 0$. In this limit the SP describes the capacity and balanced capacity. We note that for $\kappa_{\text{out}} = \kappa_{\text{in}} = 0$, Δ (and, as a result $\alpha_{\text{c}}^{\text{Unconst.}}$) is independent of all the other order parameters, simplifying the equations. In this case, we have only two coupled SP equations (for the order parameters B, C and θ), given by

$$\left(1 - \frac{\sigma_{\text{exc}} B \theta}{\bar{x}_{\text{exc}} \sqrt{2CN}} \right)^2 C = f_{\text{exc}} \gamma_+ (B) + (1 - f_{\text{exc}}) \gamma_- (B\phi) \tag{S.34}$$

$$\frac{\sigma_{\text{exc}} \theta}{\bar{x}_{\text{exc}} \sqrt{N}} = -\frac{f_{\text{exc}} \gamma_+' (B) + (1 - f_{\text{exc}}) \phi \gamma_-' (B\phi)}{\sqrt{2C}} \tag{S.35}$$

45

where we defined the functions:

$$\gamma_\pm(x) = \frac{x^2+1}{2} - \frac{1}{2}\int Du\,(x+u)^2\,\Theta\left[\pm(x+u)\right] \tag{S.36}$$

$$\gamma'_\pm(x) = x - \int Du\,(x+u)\,\Theta\left[\pm(x+u)\right]\ . \tag{S.37}$$

For the balanced SP equations we have $\theta = V_{\mathrm{th}}/\left(\sigma_{\mathrm{exc}}\Gamma\sqrt{Q}\right)$ and for the unbalanced SP equations, eq. S.28 reduces to $B=0$. Finally, α is given by (S.31).

For the unbalanced set $(B=0)$ we have $\gamma_\pm(0) = \frac{1}{2} - \frac{1}{2}\int_0^\infty Du\,(u)^2 = \frac{1}{4}$ and $\gamma'_\pm(0) = \mp\int_0^\infty Du\,(u) = \mp\frac{1}{\sqrt{\pi}}$. We immediately get $C = \frac{1}{4}$ and

$$\theta = \sqrt{\frac{2N}{\pi}}\left[f_{\mathrm{exc}}/\mathrm{CV}_{\mathrm{exc}} - (1-f_{\mathrm{exc}})/\mathrm{CV}_{\mathrm{inh}}\right]\ . \tag{S.38}$$

This solution suggests that at capacity the solutions are unbalanced $\left(\theta \sim \sqrt{N} \Rightarrow |\boldsymbol{w}| \sim 1/\sqrt{N}\right)$ and that capacity as a function of f_{exc} is constant with

$$\alpha_{\mathrm{c}} = \frac{1}{2}\alpha_{\mathrm{c}}^{\mathrm{Unconst.}}\ . \tag{S.39}$$

However, this solution is only valid as long as $\theta > V_{\mathrm{th}}/\left(\sigma_{\mathrm{exc}}\Gamma\sqrt{Q}\right)$ which is true only as long as

$$\left[f_{\mathrm{exc}}/\mathrm{CV}_{\mathrm{exc}} - (1-f_{\mathrm{exc}})/\mathrm{CV}_{\mathrm{inh}}\right] > 0 \tag{S.40}$$

which implies

$$f_{\mathrm{exc}} > f_{\mathrm{exc}}^\star = \frac{\mathrm{CV}_{\mathrm{exc}}}{\mathrm{CV}_{\mathrm{exc}} + \mathrm{CV}_{\mathrm{inh}}}\ . \tag{S.41}$$

For the solution for the balanced set $(\theta = V_{\mathrm{th}}/\left(\sigma_{\mathrm{exc}}\Gamma\sqrt{Q}\right))$ terms with $\theta/\sqrt{N}$ can be neglected and we have the equation

$$0 = f_{\mathrm{exc}}\gamma'_+(B) + (1-f_{\mathrm{exc}})\,\phi\gamma'_-(B\phi) \tag{S.42}$$

for the order parameter B. C and Q are given by

$$C = f_{\mathrm{exc}}\gamma_+(B) + (1-f_{\mathrm{exc}})\,\gamma_-(B\phi) \tag{S.43}$$

$$Q = \frac{f_{\mathrm{exc}}\gamma_+(B) + (1-f_{\mathrm{exc}})\,\gamma_-(B\phi)}{f_{\mathrm{exc}}\gamma_+(B) + \left(\frac{1-f_{\mathrm{exc}}}{\lambda^2}\right)\gamma_-(B\phi)} \tag{S.44}$$

This solution gives us the balanced capacity line

$$\alpha_{\mathrm{b}}(f_{\mathrm{exc}}) = 2\left[f_{\mathrm{exc}}\gamma_+(B) + (1-f_{\mathrm{exc}})\,\gamma_-(B\phi)\right]\alpha^{\mathrm{Unconst.}}(p_{\mathrm{out}}) \tag{S.45}$$

where B is given by the solution of (S.42) and $\alpha^{\mathrm{Unconst.}}(p_{\mathrm{out}})$ is given by (S.32) and (S.30) with $\tilde{K} = 0$.

7.3   Detailed solutions of the saddle point equations

Below we provide the saddle point equations and their solutions under various conditions. We also provide the derived form of the distributions of synaptic weights for critical solutions.

46

7.3.1 The general saddle point equations

We define the following:

$$\mathcal{F}_h = p_{\text{out}} \int Dt \ln H \left[-X_+ \left(t \right) \right] + \left(1 - p_{\text{out}} \right) \int Dt \ln H \left[X_- \left(t \right) \right] \tag{S.46}$$

$$Dt = \frac{e^{-\frac{t^2}{2}}}{\sqrt{2\pi}} dt \tag{S.47}$$

$$H \left(x \right) = \int_x^\infty Dt \tag{S.48}$$

$$X_\pm \left(t \right) = \frac{\sqrt{q} t - \Delta \mp \tilde{K}}{\sqrt{1 - q}} \tag{S.49}$$

$$\tilde{K}_{\text{in}} = \kappa_{\text{in}} / \sqrt{Q} \tag{S.50}$$

$$\tilde{K}_{\text{out}} = \theta \kappa_{\text{out}} \tag{S.51}$$

$$\phi_+ = 1, \ \phi_- = \phi \tag{S.52}$$

$$\lambda_+ = 1, \ \lambda_- = \lambda \tag{S.53}$$

$$f_+ = f_{\text{exc}}, \ f_- = 1 - f_{\text{exc}} \tag{S.54}$$

$$\alpha = \frac{P}{N} \tag{S.55}$$

$$\tilde{\theta} = \frac{\sigma_{\text{exc}} \left(\theta - \Delta \right)}{\bar{x}_{\text{exc}} \sqrt{N}} \tag{S.56}$$

$$Z_\pm = 2C \left[2C - \sqrt{2C} B \tilde{\theta} + \left(1 - q \right) \left(1 - 2\alpha Q \frac{\partial \mathcal{F}_h}{\partial Q} \left(1 - \frac{Q}{\lambda_\pm^2} \right) \right) \right]^{-1} \tag{S.57}$$

$$\Phi_\pm \left(x, z, q \right) = \frac{z \left(x^2 + 1 \right)}{2} + \frac{1 - q}{2} \left[1 + \int Du J_1 \left(\pm \frac{\sqrt{z} \left(x + u \right)}{\sqrt{\left(1 - q \right)}} \right) \right] \tag{S.58}$$

$$\Phi'_\pm \left(x, z, q \right) = zx \pm \sqrt{z \left(1 - q \right)} \int Du J_2 \left(\pm \frac{\sqrt{z} \left(x + u \right)}{\sqrt{\left(1 - q \right)}} \right) \tag{S.59}$$

$$J_1 \left(x \right) = \frac{H' \left(x \right)}{H \left(x \right)} x \tag{S.60}$$

$$J_2 \left(x \right) = \frac{H' \left(x \right)}{H \left(x \right)} \tag{S.61}$$

The saddle point equations are given by:

$$C/Q = \sum_{\pm} \frac{f_{\pm}}{\lambda_{\pm}^2} Z_{\pm} \Phi_{\pm} \left(B\phi, Z_{\pm}, q\right) \tag{S.62}$$

$$C = \sum_{\pm} f_{\pm} Z_{\pm} \Phi_{\pm} \left(B\phi_{\pm}, Z_{\pm}, q\right) \tag{S.63}$$

$$\sqrt{2C}\tilde{\theta} = -\sum_{\pm} f_{\pm} \phi_{\pm} \Phi_{\pm}' \left(B\phi_{\pm}, Z_{\pm}, q\right) \tag{S.64}$$

$$\alpha = -\frac{C}{(1-q)^2} \left(\frac{\partial \mathcal{F}_h}{\partial q}\right)^{-1} \tag{S.65}$$

$$\frac{\sigma_{\mathrm{exc}} B}{\bar{x}_{\mathrm{exc}} \sqrt{2CN}} = -\frac{1}{2(1-q)} \frac{\partial \mathcal{F}_h}{\partial \Delta} \left(\frac{\partial \mathcal{F}_h}{\partial q}\right)^{-1} \tag{S.66}$$

$$\frac{\sigma_{\mathrm{exc}} B}{\bar{x}_{\mathrm{exc}} \sqrt{2CN}} = \frac{1-q}{2\theta C} + \frac{1}{2(1-q)} \frac{\partial \mathcal{F}_h}{\partial \theta} \left(\frac{\partial \mathcal{F}_h}{\partial q}\right)^{-1} \ \textbf{OR} \ \theta = \frac{V_{\mathrm{th}}}{\sigma_{\mathrm{exc}} \Gamma \sqrt{Q}} \tag{S.67}$$

It is important to note the relation between θ and $\tilde{\theta}$. $\tilde{\theta}$ is of the order of $\theta/\sqrt{N}$ (Δ remains of order 1 under all conditions). Thus, for unbalanced solutions $\theta \sim \sqrt{N}$ and $\tilde{\theta}$ is of $\mathcal{O}(1)$ while for balanced solutions θ is of $\mathcal{O}(1)$ and $\tilde{\theta}$ is of $\mathcal{O}\left(1/\sqrt{N}\right)$ and can be neglected.

7.3.2 Saddle point equations for typical solutions

For typical solutions we solve the saddle point equations for $\kappa_{\mathrm{in}} = 0$ or $\kappa_{\mathrm{out}} = 0$ leading to $K = 0$. In this case we have $\frac{\partial \mathcal{F}_h}{\partial \theta} = \frac{\partial \mathcal{F}_h}{\partial Q} = 0$ and thus

$$Z_{\pm} = 2C \left[2C - \sqrt{2C} B\tilde{\theta} + (1-q)\right]^{-1} \tag{S.68}$$

and the saddle point equation for θ is

$$\frac{\sigma_{\mathrm{exc}} \sqrt{2C} B\theta}{\bar{x}_{\mathrm{exc}} \sqrt{N}} = 1 - q \ \textbf{OR} \ \theta = \frac{V_{\mathrm{th}}}{\sigma_{\mathrm{exc}} \Gamma \sqrt{Q}} \tag{S.69}$$

We now can solve the saddle point equations for the unbalanced case with:

$$Z_{\pm} = 1 \text{ and } \theta > \frac{V_{\mathrm{th}}}{\sigma_{\mathrm{exc}} \Gamma \sqrt{Q}}, \ \tilde{\theta} > 0 \tag{S.70}$$

and for the balanced case with

$$Z_{\pm} = 2C \left[2C + (1-q)\right]^{-1} \text{ and } \theta = \frac{V_{\mathrm{th}}}{\sigma_{\mathrm{exc}} \Gamma \sqrt{Q}}, \ \tilde{\theta} = 0 \tag{S.71}$$

We find that for $\alpha < \alpha_{\mathrm{b}}$ a solution only exist for equations of the balanced case while for $\alpha > \alpha_{\mathrm{b}}$ a solution exist for the equations for the unbalanced case. Thus typical solutions are balanced below α_{b} and unbalanced above it. The norm of the weight and the imbalance index depicted in Fig. 2b and Fig. 2c are given by

$$|\boldsymbol{w}| = \frac{1}{\sqrt{Q}\theta} \tag{S.72}$$

$$\mathrm{IB} = \frac{\sum_{\pm} f_{\pm} \phi_{\pm} \Phi_{\pm}' \left(B\phi_{\pm}, Z, q\right)}{\sum_{\pm} \pm f_{\pm} \phi_{\pm} \Phi_{\pm}' \left(B\phi_{\pm}, Z, q\right)} \tag{S.73}$$

48

7.3.3 Solutions with significant κ_{out} are balanced

In this section we show that all unbalanced solutions have output robustness of order $1/\sqrt{N}$ and, equivalently, Solutions with κ_{out} of order 1 are balanced.

Theorem: All Unbalanced solutions have output robustness of the order of $1/\sqrt{N}$.

Proof: In the case of output robustness we $\tilde{K} = \tilde{K}_{\text{out}} = \theta \kappa_{\text{out}}$ and thus, $\frac{\partial \mathcal{F}_h}{\partial Q} = 0$. We are looking for unbalanced solutions ($\tilde{\theta} > 0$, $\theta \sim \mathcal{O}\left(\sqrt{N}\right)$) so we have the equations,

$$\frac{\sigma_{\text{exc}} B}{\bar{x}_{\text{exc}} \sqrt{2CN}} = -\frac{1}{2(1-q)} \frac{\partial \mathcal{F}_h}{\partial \Delta} \left(\frac{\partial \mathcal{F}_h}{\partial q}\right)^{-1} \tag{S.74}$$

$$\frac{\sigma_{\text{exc}} B}{\bar{x}_{\text{exc}} \sqrt{2CN}} = \frac{1-q}{2\theta C} + \frac{1}{2(1-q)} \frac{\partial \mathcal{F}_h}{\partial \theta} \left(\frac{\partial \mathcal{F}_h}{\partial q}\right)^{-1} . \tag{S.75}$$

Both equations must be satisfied therefore we have (using (S.65), (S.74) and (S.75))

$$0 = \frac{\partial \mathcal{F}_h}{\partial \Delta} + \frac{\partial \mathcal{F}_h}{\partial \theta} - \frac{1}{\alpha \theta} \tag{S.76}$$

Performing the derivatives we get

$$0 = (\kappa_{\text{out}} + 1) p_{\text{out}} \int Dt J_2 (-X_+) + (\kappa_{\text{out}} - 1)(1 - p_{\text{out}}) \int Dt J_2 (X_-) - \frac{\sqrt{1-q}}{\alpha \theta} \tag{S.77}$$

Now, we use eq. S.74, leading to

$$p_{\text{out}} \int Dt J_2 (-X_+) = (1 - p_{\text{out}}) \int Dt J_2 (X_-) - M/\sqrt{N} \tag{S.78}$$

where we defined M as

$$M = \frac{\sqrt{2} B \sigma_{\text{exc}} \sqrt{1-q}}{\sqrt{C} \bar{x}_{\text{exc}}} \frac{\partial \mathcal{F}_h}{\partial q} \tag{S.79}$$

which remains of $\mathcal{O}(1)$. Thus, we are left with

$$0 = 2\kappa_{\text{out}} (1 - p_{\text{out}}) \int Dt J_2 (X_-) - (\kappa_{\text{out}} + 1) \frac{M}{\sqrt{N}} - \frac{\sqrt{1-q}}{\alpha \theta} \tag{S.80}$$

Note that $J_2(x) < 0$ and the first term is negative (non zero). The other two terms scale as $1/\sqrt{N}$ and therefore the equation can be satisfied only if $\kappa = \frac{\kappa_0}{\sqrt{N}}$ ∎

7.3.4 Saddle point equations for critical solutions

To find the capacity, balanced capacity and solutions with maximal output and input robustness we consider the limit $q \to 1$.

We define,

$$G_Q = \lim_{q \to 1} \frac{Q}{(1-q)} \left(\frac{\partial \mathcal{F}_h}{\partial q}\right)^{-1} \frac{\partial \mathcal{F}_h}{\partial Q} , \tag{S.81}$$

49

thus in this limit $Z_\pm$ is given by:

$$Z_\pm = \left[1 - \frac{B\tilde{\theta}}{\sqrt{2C}} + \left(1 - \frac{Q}{\lambda_\pm^2}\right) G_Q\right]^{-1} . \tag{S.82}$$

In addition,

$$\lim_{q \to 1} \Phi_\pm(x, z, q) = z\gamma_\pm(x) \tag{S.83}$$

$$\gamma_\pm(x) = \frac{x^2 + 1}{2} - \frac{1}{2} \int Du \, (x + u)^2 \, \Theta\left[\pm (x + u)\right] \tag{S.84}$$

$$\lim_{q \to 1} \Phi'_\pm(x, z, q) = z\gamma'_\pm(x) \tag{S.85}$$

$$\gamma'_\pm(x) = x - \int Du \, (x + u) \, \Theta\left[\pm (x + u)\right] , \tag{S.86}$$

and, in the $q \to 1$ limit we have:

$$(1 - q) \frac{\partial \mathcal{F}_h}{\partial \Delta} = M\left(\Delta, \tilde{K}\right) \tag{S.87}$$

$$M\left(\Delta, \tilde{K}\right) = p_{\text{out}} \int_{-\infty}^{\Delta + \tilde{K}} Dt \left(t - \Delta - \tilde{K}\right) + (1 - p_{\text{out}}) \int_{\Delta - \tilde{K}}^{\infty} Dt \left(t - \Delta + \tilde{K}\right) \tag{S.88}$$

$$(1 - q)^2 \frac{\partial \mathcal{F}_h}{\partial q} = -\frac{1}{2} \alpha^{\text{Unconst.}}\left(\Delta, \tilde{K}\right) \tag{S.89}$$

$$\alpha^{\text{Unconst.}}\left(\Delta, \tilde{K}\right) = \left[p_{\text{out}} \int_{-\infty}^{\Delta + \tilde{K}} Dt \left(t - \Delta - \tilde{K}\right)^2 + (1 - p_{\text{out}}) \int_{\Delta - \tilde{K}}^{\infty} Dt \left(t - \Delta + \tilde{K}\right)^2\right]^{-1} . \tag{S.90}$$

We now write the final form of the saddle point equations for critical solutions:

$$C = \sum_\pm f_\pm Z_\pm^2 \gamma_\pm(B\phi_\pm) \tag{S.91}$$

$$Q = \frac{\sum_\pm f_\pm Z_\pm^2 \gamma_\pm(B\phi_\pm)}{\sum_\pm \frac{f_\pm}{\lambda_\pm^2} Z_\pm^2 \gamma_\pm(B\phi_\pm)} \tag{S.92}$$

$$\tilde{\theta} = -\frac{\sum_\pm f_\pm \phi_\pm Z_\pm \gamma'_\pm(B\phi_\pm)}{\sqrt{2 \sum_\pm f_\pm Z_\pm^2 \gamma_\pm(B\phi_\pm)}} \tag{S.93}$$

$$0 = M\left(\Delta, \tilde{K}\right) \tag{S.94}$$

$$\frac{B}{\sqrt{2CN}} = -\frac{\bar{x}_{\text{ex}}}{\sigma_{\text{ex}}} 2C\alpha^{\text{Unconst.}}\left(\Delta, \tilde{K}\right) \lim_{q \to 1} (1 - q) \frac{\partial \mathcal{F}_h}{\partial \theta} \; \boldsymbol{OR} \; \theta = \frac{V_{\text{th}}}{\sigma_{\text{exc}} \Gamma \sqrt{Q}} . \tag{S.95}$$

Finally α is given by:

$$\alpha = 2C\alpha^{\text{Unconst.}}\left(\Delta, \tilde{K}\right) \tag{S.96}$$

7.3.5 Capacity and balanced capacity

The capacity is given for $\delta = 0$ and $\kappa = 0$. In this case both $\frac{\partial \mathcal{F}_h}{\partial \theta}$ and $\frac{\partial \mathcal{F}_h}{\partial Q}$ are zero and equation S.95 has two possible solutions:

$$B = 0, \ \theta > \frac{V_{\text{th}}}{\sigma_{\text{exc}} \Gamma \sqrt{Q}} \ , \tag{S.97}$$

for unbalanced solutions **or**

$$\theta = \frac{V_{\text{th}}}{\sigma_{\text{exc}} \Gamma \sqrt{Q}}, \ \tilde{\theta} = 0 \ , \tag{S.98}$$

for balanced solutions. In both cases we have $Z_\pm = 1$.

Unbalanced solution   The saddle point equations become

$$Q = \frac{1}{\sum_\pm \frac{1}{\lambda_\pm^2} f_\pm} \tag{S.99}$$

$$\tilde{\theta} = \frac{1}{\sqrt{\pi}} \sum_\pm \pm f_\pm \phi_\pm \tag{S.100}$$

$$C = \frac{1}{4} \tag{S.101}$$

and the capacity is given by:

$$\alpha_c = \frac{1}{2} \alpha^{\text{Unconst.}} (\Delta, 0) \tag{S.102}$$

where Δ is given by $M(\Delta, 0) = 0$.

This solution is valid only when θ is larger than its $\mathcal{O}(1)$ lower bound which is guarantied in the large N limit as long as $\tilde{\theta} > 0$. Using eq. S.100, this entails that

$$f_{\text{exc}} > f_{\text{exc}}^\star \tag{S.103}$$

with

$$f_{\text{exc}}^\star = \frac{\phi}{1 + \phi} \tag{S.104}$$

or conversely $\phi < \frac{f_{\text{exc}}}{1 - f_{\text{exc}}}$.

Balanced solution   In this solution we have $\theta = \frac{V_{\text{th}}}{\sigma_{\text{exc}} \Gamma \sqrt{Q}}, \ \tilde{\theta} = 0$.

B is given by the solution to

$$\sum_\pm f_\pm \phi_\pm \gamma'_\pm (B\phi_\pm) = 0 \tag{S.105}$$

and we have

$$Q = \frac{\sum_\pm f_\pm \gamma_\pm (B\phi_\pm)}{\sum_\pm \frac{1}{\lambda_\pm^2} f_\pm \gamma_\pm (B\phi_\pm)} \tag{S.106}$$

51

$$C = \sum_{\pm} f_{\pm} \gamma_{\pm} \left(B\phi_{\pm} \right) \tag{S.107}$$

and

$$\alpha_{\mathrm{b}} = 2C\alpha^{\mathrm{Unconst.}} \left(\Delta, 0 \right) \tag{S.108}$$

where Δ is given by $M\left(\Delta, 0 \right) = 0$.

This gives the balanced capacity line. For $f_{\mathrm{exc}} < f_{\mathrm{exc}}^{\star}$ this is the capacity line as well. Thus, for $f_{\mathrm{exc}} < f_{\mathrm{exc}}^{\star}$, at capacity the solution is balanced.

7.3.6 Coexistence of balanced and unbalanced solutions below the balanced capacity line

To show that unbalanced solutions coexist with balanced solutions for any $\alpha < \alpha_{\mathrm{b}}$, we calculate the capacity of unbalanced solutions with a given norm. This can be done by solving equations (S.91)-(S.94) while imposing the condition $|\boldsymbol{w}| = \frac{V_{\mathrm{thr}} W}{\sqrt{N} \sigma_{\mathrm{exc}}}$ through the saddle point equation of θ:

$$\theta = \frac{\sqrt{N}}{W \sqrt{Q}} \ . \tag{S.109}$$

We therefor have:

$$\tilde{\theta} = \frac{\sigma_{\mathrm{exc}} \left(\theta - \Delta \right)}{\bar{x}_{\mathrm{exc}} \sqrt{N}} \simeq \frac{\sigma_{\mathrm{exc}}}{\bar{x}_{\mathrm{exc}} W \sqrt{Q}} = \frac{1}{\tilde{W} \sqrt{Q}} \tag{S.110}$$

We are interested in the capacity and therefor we take $K = 0$. As a results we have:

$$Z_{\pm} = \left[1 - \frac{B}{\sqrt{2CQ\tilde{W}^2}} \right]^{-1} \tag{S.111}$$

and the saddle point equations become:

$$\frac{1}{\tilde{W}} = -\frac{\sum_{\pm} f_{\pm} \phi_{\pm} \gamma'_{\pm} \left(B\phi_{\pm} \right)}{\sqrt{2 \sum_{\pm} \frac{f_{\pm}}{\lambda_{\pm}^2} \gamma_{\pm} \left(B\phi_{\pm} \right)}} \tag{S.112}$$

$$C = \left[1 - \frac{B}{\tilde{W} \sqrt{2CQ}} \right]^{-2} \sum_{\pm} f_{\pm} \gamma_{\pm} \left(B\phi_{\pm} \right) \tag{S.113}$$

$$0 = M\left(\Delta, 0 \right) \tag{S.114}$$

where Q is given by

$$Q = \frac{\sum_{\pm} f_{\pm} \gamma_{\pm} \left(B\phi_{\pm} \right)}{\sum_{\pm} \frac{f_{\pm}}{\lambda_{\pm}^2} \gamma_{\pm} \left(B\phi_{\pm} \right)} \tag{S.115}$$

Given the value of B and Q the equation for C can be solved for $\sqrt{C}$ and we get:

$$\sqrt{C} = \frac{B}{\sqrt{2Q}\tilde{W}} + \sqrt{\sum_{\pm} f_{\pm} \gamma_{\pm} \left(B\phi_{\pm} \right) - \left(\frac{B}{\sqrt{2Q}\tilde{W}} \right)^2} \tag{S.116}$$

This solution is valid as long as $\sqrt{C} \geq 0$. The conditional capacity $\alpha_{\rm c}\left(\tilde{W}\right)$ is then given by

$$\alpha_{\rm c}\left(\tilde{W}\right) = 2C\alpha^{\rm Unconst.}\left(\Delta, 0\right) \ . \tag{S.117}$$

It is easy to see that for $\tilde{W} \to \infty$, the saddle point equations converge to the equations of the balanced capacity and thus $\alpha_{\rm c}\left(\tilde{W}\right)$ approaches $\alpha_{\rm b}$. In addition we find that for $f_{\rm exc} < f_{\rm exc}^{\star}$, $\alpha_{\rm c}\left(\tilde{W}\right)$ is a monotonically increasing function of $\tilde{W}$. Another way to interpret this result is to 'invert the function' and ask what is the minimal value of $\tilde{W}$ that permits solutions given α. Our result implies that strictly below $\alpha_{\rm b}$ the minimal value of $\tilde{W}$ that permits solutions is of $\mathcal{O}\left(1\right)$ (i.e. $|\boldsymbol{w}|$ of $\mathcal{O}\left(1/\sqrt{N}\right)$) and unbalanced solutions exist. The minimal $\tilde{W}$ diverges as α approaches $\alpha_{\rm b}$ and hence the solution at $\alpha_{\rm b}$ is balanced ($|\boldsymbol{w}|$ of $\mathcal{O}\left(1\right)$).

7.3.7 Saddle point equations for the maximal $\kappa_{\rm in}$ solution

In this case we have $\tilde{K} = \tilde{K}_{\rm in} = \frac{\delta}{\sqrt{Q}}$ and therefore $\frac{\partial \mathcal{F}_h}{\partial \theta} = 0$. For unbalanced solutions we have

$$B = 0, \ \theta > \frac{V_{\rm th}}{\sigma_{\rm exc}\Gamma\sqrt{Q}}, \ \tilde{\theta} > 0 \tag{S.118}$$

and for balanced solutions we have

$$\theta = \frac{V_{\rm th}}{\sigma_{\rm exc}\Gamma\sqrt{Q}}, \ \tilde{\theta} = 0 \ . \tag{S.119}$$

In both cases $Z_{\pm}$ is given by

$$Z_{\pm} = \left[1 + \left(1 - \frac{Q}{\lambda_{\pm}^2}\right)G_Q\right]^{-1} \tag{S.120}$$

with

$$G_Q = \kappa_{\rm in}/\sqrt{Q}\,\alpha^{\rm Unconst.}\left(\Delta, \kappa_{\rm in}/\sqrt{Q}\right)\left[p_{\rm out}\int_{-\infty}^{\Delta + \frac{\kappa_{\rm in}}{\sqrt{Q}}} Dt\left(t - \Delta - \frac{\kappa_{\rm in}}{\sqrt{Q}}\right)\right. \tag{S.121}$$

$$\left. - (1 - p_{\rm out})\int_{\Delta - \frac{\kappa_{\rm in}}{\sqrt{Q}}}^{\infty} Dt\left(t - \Delta + \frac{\kappa_{\rm in}}{\sqrt{Q}}\right)\right]$$

Unbalanced solution In this case we have equations for Δ and Q:

$$M\left(\Delta, \kappa_{\rm in}/\sqrt{Q}\right) = 0 \tag{S.122}$$

$$Q = \frac{\sum_{\pm} f_{\pm}Z_{\pm}^2}{\sum_{\pm} \frac{1}{\lambda_{\pm}^2}f_{\pm}Z_{\pm}^2} \ . \tag{S.123}$$

We then have:

$$\tilde{\theta} = \frac{\frac{1}{\sqrt{2\pi}} \sum_{\pm} \pm f_{\pm} \phi_{\pm} Z_{\pm}}{\sqrt{\frac{1}{2} \sum_{\pm} f_{\pm} Z_{\pm}^2}} \tag{S.124}$$

$$C = \frac{1}{4} \sum_{\pm} f_{\pm} Z_{\pm}^2 \tag{S.125}$$

and

$$\alpha = 2C\alpha^{\text{Unconst.}} \left(\Delta, \kappa_{\text{in}}/\sqrt{Q} \right) \tag{S.126}$$

Balanced solution In this case we have equations for Δ, B and Q:

$$M \left(\Delta, \kappa_{\text{in}}/\sqrt{Q} \right) = 0 \tag{S.127}$$

$$Q = \frac{\sum_{\pm} f_{\pm} \gamma_{\pm} (B\phi_{\pm}) Z_{\pm}^2}{\sum_{\pm} \frac{1}{\lambda_{\pm}^2} f_{\pm} \gamma_{\pm} (B\phi_{\pm}) Z_{\pm}^2} \tag{S.128}$$

$$0 = \sum_{\pm} f_{\pm} \phi_{\pm} \gamma'_{\pm} (B\phi_{\pm}) Z_{\pm} \tag{S.129}$$

the equations for G_Q (S.121) and α (S.126) remain the same, however C is given by:

$$C = \sum_{\pm} f_{\pm} \gamma_{\pm} (B\phi_{\pm}) Z_{\pm}^2 \tag{S.130}$$

Transition between balanced and unbalanced solutions Transition points between balanced and unbalanced solutions depend on the value of ϕ, λ and f_{exc}. Transition points are points in which both $B = 0$ and $\tilde{\theta} = 0$. Thus we have

$$\phi^{\star} = \frac{f_{\text{exc}} Z_+}{(1 - f_{\text{exc}}) Z_-} \tag{S.131}$$

where Q and Δ are given by (S.123) and (S.122). Thus $\phi^{\star}$ is a function of κ_{in} and λ. Solutions are balanced for $\phi > \phi^{\star}$ and unbalanced for $\phi < \phi^{\star}$ [Fig. S2b].

7.3.8 Saddle point equations for the maximal κ_{out} solution

Unbalanced solution This solution is valid for $\alpha > \alpha_{\text{b}}$, $f_{\text{exc}} > f_{\text{exc}}^{\star}$. We look for a solution with $\tilde{\theta} > 0$ thus θ must scale as $\sqrt{N}$.

In this case $\tilde{K} = \theta \kappa$ and so $\frac{\partial \mathcal{F}_h}{\partial Q} = 0$ and $Z_{\pm} = \left[1 - \frac{B\tilde{\theta}}{\sqrt{2C}} \right]^{-1}$.

We then have:

$$Q = \frac{\sum_{\pm} f_{\pm} \gamma_{\pm} (B\phi_{\pm})}{\sum_{\pm} \frac{1}{\lambda_{\pm}^2} f_{\pm} \gamma_{\pm} (B\phi_{\pm})} \tag{S.132}$$

And we are left with equations to solve for $\tilde{\theta}$, B and Δ.

$$\tilde{\theta} = -\frac{\sum_{\pm} f_{\pm} \phi_{\pm} \gamma'_{\pm} (B\phi_{\pm})}{\sqrt{2 \sum_{\pm} f_{\pm} \gamma_{\pm} (B\phi_{\pm})}} \tag{S.133}$$

$$M\left(\Delta, \tilde{K}\right) = 0 \tag{S.134}$$

and

$$\frac{B}{\sqrt{2CN}} = -\frac{\bar{x}_{\text{ex}}}{\sigma_{\text{ex}}} \kappa \alpha^{\text{Unconst.}}\left(\Delta, \tilde{K}\right) \left[f \int_{-\infty}^{\Delta+\tilde{K}} Dt \left(t - \Delta - \tilde{K}\right) - (1-f) \int_{\Delta-\tilde{K}}^{\infty} Dt \left(t - \Delta + \tilde{K}\right) \right] \tag{S.135}$$

There is only a solution if

$$\kappa = \frac{\sigma_{\text{exc}}}{\bar{x}_{\text{exc}}\sqrt{N}} \kappa_0, \ \theta \simeq \sqrt{N} \frac{\bar{x}_{\text{ex}}}{\sigma_{\text{ex}}} \tilde{\theta} \tag{S.136}$$

so we have $\tilde{K} = \tilde{\theta}\kappa_0$ and

$$\frac{B}{\sqrt{2C}} = -\kappa_0 \alpha^{\text{Unconst.}}\left(\Delta, \tilde{\theta}\kappa_0\right) \left[f \int_{-\infty}^{\Delta+\tilde{\theta}\kappa_0} Dt \left(t - \Delta - \tilde{\theta}\kappa_0\right) - (1-f) \int_{\Delta-\tilde{\theta}\kappa_0}^{\infty} Dt \left(t - \Delta + \tilde{\theta}\kappa_0\right) \right] . \tag{S.137}$$

Finally we have $C = Z^2 \sum_{\pm} f_{\pm} \gamma_{\pm} (B\phi_{\pm})$, from which we can isolate C to have

$$C = \left[\sum_{\pm} f_{\pm} \gamma_{\pm} (B\phi_{\pm}) \right] \left[1 - \frac{B \sum_{\pm} f_{\pm} \phi_{\pm} \gamma'_{\pm} (B\phi_{\pm})}{2 \sum_{\pm} f_{\pm} \gamma_{\pm} (B\phi_{\pm})} \right]^2 . \tag{S.138}$$

α is given as before $\alpha = 2C\alpha^{\text{Unconst.}}\left(\Delta, \tilde{\theta}\kappa_0\right)$.

The equations given in this section are equivalent to the ones derived in [26].

Balanced solution   We look for balanced solutions with $\theta = \frac{V_{\text{th}}}{\sigma_{\text{exc}}\Gamma\sqrt{Q}}$, $\tilde{\theta} = 0$. The saddle point equations in this case are given by the same equations as the balanced solution described in subsection 7.3.7 with $\kappa_{\text{out}} V_{\text{th}}/\sigma_{\text{exc}}\Gamma$ replacing κ_{in}.

7.3.9   Distribution of synaptic weights

We derive the mean distribution of synaptic weights for critical solutions $(q \to 1)$

$$P_{\pm}(w) = H\left(\mp B\phi_{\pm}\right) \delta(w) + \sqrt{\frac{\theta^2 N \lambda_{\pm}^2}{2\pi\sigma_{w\pm}^2}} \exp\left[-\frac{\left(\theta\sqrt{N}\lambda_{\pm}w + B\phi_{\pm}\sigma_{w\pm}\right)^2}{2\sigma_{w\pm}^2} \right] , \tag{S.139}$$

with $\sigma_{w\pm} = \frac{Z_{\pm}}{\sqrt{2C}}$, where P_+ and P_- denote the probability densities for excitatory and inhibitory synaptic weights respectively, $\delta(x)$ is the Dirac delta function and weights are given in units of $V_{\text{th}}/\sigma_{\text{exc}}$. The fraction of silent synapses is given by $H(-B)$ for excitatory synapses and by $H(B\phi)$ for inhibitory synapses.